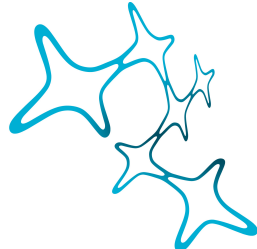


LUDWIG-MAXIMILIANS-UNIVERSITÄT  
MÜNCHEN

FACULTY OF BIOLOGY, COMPUTATIONAL NEUROSCIENCE



Graduate School of  
Systemic Neurosciences  
LMU Munich

MASTER'S THESIS

---

Computational Simulation of  
Time Perception

---

Katharina M BRACHER

Supervision: Dr. Kay THURLEY  
Prof. Dr. Andreas HERZ

## Abstract

Timing in the brain is thought to be encoded through state dynamics of neuronal populations. Experimentally, reproduction tasks are a useful approach to study sensory processing of time because a relationship between external events and their internal perception is established. In such experiments, behavioral responses are characterized by specific biases such as the regression effect, i.e. the overestimation of small time intervals and the underestimation of large ones. This effect is thought to result from error minimization strategies underlying the behavioral responses. However, how the brain implements such optimal statistical processing is unknown. Here, I investigate a neural circuit model that has been proposed recently to explain various timing behaviors, and apply it to realistic time reproduction experiments. Parameters that yield minimal behavioral error predict the characteristic behavioral effects.

Using these parameters, I further investigate the effects of stimulus statistics on behavior and find that the model predicts an influence of the mean of the stimulus, but not of its variance, on behavior. These results are in line with data from behavioral experiments with gerbils. Some animals, however, increase their performance in cases of high variance stimuli, suggesting an adaptation of dynamics to stimulus statistics. This work provides further evidence that a dynamical systems perspective has the potential to explain timing.

# Contents

<b>1</b>	<b>Introduction</b>	<b>1</b>
1.1	Behavioral Effects in Magnitude Estimation . . . . .	1
1.2	Time Estimation via Predictive Timing . . . . .	2
1.3	Brain Dynamics Underlying Time Perception . . . . .	3
<b>2</b>	<b>A Circuit Model for Time Estimation</b>	<b>5</b>
2.1	Basic Circuit . . . . .	5
2.2	Extended Circuit for Experiment Simulation . . . . .	6
<b>3</b>	<b>Model Parameters for Error Minimization</b>	<b>11</b>
3.1	Behaviorally Plausible Time Reproductions . . . . .	11
3.2	Model Regime for Error-Minimized Behavior . . . . .	12
3.3	High Input Regime . . . . .	13
<b>4</b>	<b>General Underestimation of Reproductions</b>	<b>18</b>
4.1	Time Constant and Delay Influence Reproductions . . . . .	18
4.2	Adjusted Experiment Simulation . . . . .	19
<b>5</b>	<b>Influence of External Variability on Behavior</b>	<b>20</b>
5.1	Optimality Predicts Key Effects . . . . .	21
5.2	Optimality Predicts no Effect of Variance on Behavior . . . . .	23
5.3	Comparison of Model Output to Real Data . . . . .	23
<b>6</b>	<b>Discussion</b>	<b>26</b>
6.1	Representation of Stimulus Statistics . . . . .	27
6.2	Scales of Timing . . . . .	28
6.3	Integration into Classical and Bayesian Framework . . . . .	29
	<b>Supplements</b>	<b>31</b>
	<b>References</b>	<b>40</b>

# 1 Introduction

Animals are capable of producing complex and flexible behaviors that rely on the interplay between motor and sensory systems. Timing is critical for many of these sensorimotor functions, ensuring the ability to anticipate and coordinate interactions with the environment. Sensory and motor timing in the millisecond range is particularly important, as this timescale includes temporal cues for vocalization as well as fine motor coordination. However, there is no sensory organ responsible for time perception, which means that perception must be generated internally by extracting information from sensory inputs. Although time is pervasive in animal behavior, it is elusive and difficult to study. The neural implementation that allows the brain to perceive and internally perform complex temporal computations remains unknown. But the mechanism of timing might provide powerful insights into general mechanisms of cognition and neural computations (Issa et al. 2020).

Magnitude estimation is a useful approach to explore sensory processing because it involves establishing a relationship between external events and their internal perception, for example, by evaluating or reproducing a time interval. However, perception of time is affected by noise arising from internal, neural representations of externally-derived inputs, which themselves are subject to noise due to variability in the environment. A variety of experimental studies have found characteristic behavioral effects in magnitude estimation that might arise to minimize errors in the presence of noise (Petzschner et al. 2015).

In the following, key effects of magnitude estimation are discussed. I then summarize evidence for brain dynamics underlying time perception and introduce a model to simulate time perception.

## 1.1 Behavioral Effects in Magnitude Estimation

Magnitude estimation exhibits characteristic effects across sensory modalities. The most striking observation is regression to the mean of stimuli. In other words, small stimuli are overestimated whereas large stimuli are underestimated (*regression or central tendency effect*). This effect intensifies for ranges with larger stimuli (*range effect*). Additionally, the standard deviation of estimates increases monotonically for larger stimuli (*scalar variability*). Finally, the recent history of presentation influences the current stimuli estimation (*sequential effects*). All effects mentioned above are displayed in Fig. 1. Modality-independence of these effects suggests the existence of a common underlying principle or processing mechanisms that would, for example, explain an optimal strategy for unreliable judgments due to noise. Minimizing errors in judgment can be achieved by integrating prior experience with immediate sensory input.

Therefore, this is often described by Bayesian models. In these models, sensory information is represented by a likelihood function and is combined with prior experience, resulting in biased estimates (Knill and Pouget 2004). Ongoing research is trying to identify neural mechanisms behind such behavior.

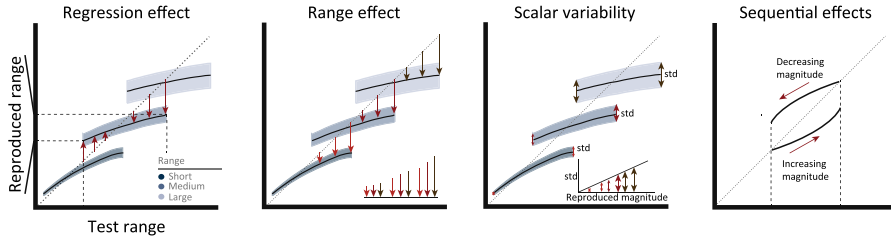


Figure 1: **Behavioral effects.** *Regression effect*: in a distribution of stimuli, large stimuli are underestimated, and small stimuli are overestimated, which results in a regression to the mean of the range. *Range effect*: the regression to the mean gets more pronounced for ranges that comprise larger stimuli. *Scalar variability*: the standard deviation of the reproduced magnitude grows linearly with larger estimates. *Sequential effects*: the history of presented stimuli (e.g. ascending or descending order) influences the reproduced magnitude. (Adapted from Petzschner et al. 2015, reproduced with permission from F. Petzschner.)

## 1.2 Time Estimation via Predictive Timing

Experiments, in which subjects have to measure and reproduce time intervals, allow us to study how the brain integrates expectations with current sensory input in order to achieve correct timing. Time reproduction is usually accomplished by at least one presentation of the time interval e.g. between two external events (*sensory timing*), and a reproduction period that is indicated by the subject's response (*motor timing*). In both epochs elapsed time needs to be estimated; the difference lies in the termination of the interval. In sensory timing, the time interval is terminated by an external event, while in motor timing, completion is internally generated and executed by the subject's response (Grondin 2010).

Time between two events can be measured in an absolute or predictive manner. In the case of absolute timing, time can be continuously estimated by integration of ticks from a central clock (Buhusi and Meck 2005, Paton and Buonomano 2018). The rate at which activity increases does not depend on the time interval. In contrast, for predictive timing, a fixed state is reached at the end of the time interval, by adjusting the rate of a process according to the anticipated time. Recently, evidence of predictive timing has emerged, suggesting that the central nervous system makes use of predictive signaling mechanisms, allowing the animal to contemplate sensory consequences of actions (Egger et al.

2019, Meirhaeghe et al. 2021).

Predictive coding is a framework, in which the brain predicts its upcoming states and refines these predictions through error signals (Rao and Ballard 1999, Huang and Rao 2011, Ficco et al. 2021). Intrinsic neural representations of motor actions are used as predictor of sensory consequences. If there is a mismatch between predicted and actual sensory feedback, an internal model is updated by the error signal (Bubic et al. 2010, Clark 2013, Straka et al. 2018). The internal model can include a prior, to integrate expectations into the time estimate. Based on predictions and expectations, flexible control of neural mechanisms is required to measure and produce time intervals. This raises the question of how flexible control over brain dynamics can be achieved.

### 1.3 Brain Dynamics Underlying Time Perception

Increasing evidence suggests that the brain encodes time in population state dynamics. The frontal cortex is a brain area that has previously been associated with timing behavior (Shima and Tanji 2000, Lewis et al. 2004, Genovesio et al. 2006, Emmons et al. 2017, Wang et al. 2018). In time reproduction experiments, the activity of individual cells in the frontal cortex heterogeneous response profiles, many of which are temporally scaled according to the produced time interval (Remington et al. 2018, Wang et al. 2018, Sohn et al. 2019, Henke et al. 2021). Indeed, time can be encoded predictively relative to the mean of time intervals by temporal scaling activity. Scaling is a phenomenon that is consistent at the population level, when activity is displayed in a low-dimensional state space. In the state space, the activity of all neurons is represented over time by a so-called neural trajectory (Cueva et al. 2020). It has been shown that in sensory timing, population activity evolves along a common trajectory, whereas in motor timing, trajectories scale in speed to reach a common terminal state, which then triggers an action (Mita et al. 2009, Murakami et al. 2014, Wang et al. 2018, Sohn et al. 2019, Henke et al. 2021, Meirhaeghe et al. 2021). Experiments have revealed a causal link between population dynamics and time encoding. Cooling the medial prefrontal cortex in rats, slowed population dynamics down, resulting in longer time estimates (Xu et al. 2014). It could therefore be concluded that the brain dynamically changes patterns of neural activity to flexibly adjust behavior to time actions, and flexible motor timing can be achieved by controlling the speed of neural dynamics (Remington et al. 2018, Wang et al. 2018, Sohn et al. 2019, Tsao et al. 2022).

**A circuit model for time estimation.** Data indicates that neural trajectories reflect the internal estimate of a time interval and are influenced by a

prior. Experiments with multiple, consecutive stimulus presentations showed a sequential update of the estimate. This provides evidence for a predictive process that yields an error signal to correct the speed of the neural trajectory in the next epoch. Wang et al. (2018) proposed a potential neural mechanism for speed control, which involved flexibly adjusting the effective time constant of a network. In fact, the population activity reflects an interval-dependent speed command that is updated based on a mismatch between predicted and actual interval in measurement epochs (Wang et al. 2018, Egger et al. 2019).

Building on these findings, Remington et al. (2018) showed that flexible control of behavior in interval reproduction can be understood in terms of a dynamical system that is characterized by the initial state and an external input. In a two-neuron-model, which is well known for modeling decision-making (Wang 2002, Roxin and Ledberg 2008), the input level can be used to adapt the effective time constant of the system. Based on this mechanism, Egger et al. (2020) developed an extended circuit model for sensorimotor timing, which was used in interval reproduction tasks and fitted to human data that exhibited classical effects of magnitude estimation. However, different time intervals were presented separately and not in a random sequence as would be usual for classical time reproduction experiments.

**Research questions.** By applying the circuit model to simulations that reflect more realistic conditions of time reproduction experiments, the present work addresses the question of which behavioral effects can be explained by the extended circuit model. I demonstrate that simulations of realistic experiments, classical effects of magnitude estimation are reproduced by the model with parameters that minimize errors in behavior, providing further evidence that a dynamical systems perspective has the potential to explain flexible timing. Following this result, I examine how variability in stimuli affects behavior.

In the subsequent two sections, the circuit model is described in detail. I discuss different input regimes of the model and identify model parameters that minimize errors in the behavior. In Section 4, I analyze the behavior of the model and make adjustments to the experiment design to then investigate the effects of stimulus statistics on behavior in Section 5. Furthermore, I evaluate predictions of the model, and compare these to data from time reproduction experiments of gerbils and humans.

## 2 A Circuit Model for Time Estimation

The model is build on a basic circuit, which is introduced in the following. I then describe the extension of the circuit to include a mechanism for updating the external input (Egger et al. 2020). Depending on the input strength, the model operates in different regimes. In this section, I focus on the intermediate input regime, but I will discuss the high input regime in Section 3.

### 2.1 Basic Circuit

Flexible speed control can be achieved by a model consisting only of three units,  $(u, v, y)$  that represent population activity. The dynamics of  $u, v$ , and  $y$  are defined as follows:

$$\begin{aligned} \tau \frac{du}{dt} &= -u + \theta(W_{uI}I - W_{uv}v + \eta_u), \\ \tau \frac{dv}{dt} &= -v + \theta(W_{vI}I - W_{vu}u + \eta_v), \\ \tau \frac{dy}{dt} &= -y + W_{yu}u - W_{yv}v + \eta_y. \end{aligned} \quad (1)$$

Two units,  $u$  and  $v$ , receive a tonic symmetric input  $I$  ( $W_{uI} = W_{vI} = 6$ ) and are mutually inhibiting each other ( $W_{uv} = W_{vu} = 6$ ). The inputs to  $u$  and  $v$  are governed by a sigmoid activation function  $\theta(x) = \frac{1}{1+\exp(-x)}$ . The output unit  $y$  receives excitatory input from  $u$  and inhibitory input from  $v$  ( $W_{yu} = W_{yv} = 1$ ) which results in a ramp-like activity of  $y$  (Fig. 2a). Different external inputs to the sigmoid activation function, control the effective time constants of the system. Stronger inputs drive the activation more towards the saturating non-linearity, which leads to larger effective time constants. Because of this, the model yields a repertoire of slopes that can be exploited for time reproduction (Fig. 2c)(Egger et al. 2020). Stochastic synaptic inputs are modeled as independent white noise  $\eta_u, \eta_v, \eta_y$  with standard deviation  $\sigma$ . To simulate the dynamics of  $u, v, y$  and  $I$ , Euler's method was used with a step size  $\Delta t$  that corresponds to 10 ms. A description of the implementation can be found in Supplements.

**The model has three distinct input regimes.** Depending on the input  $I$ , the system shows different dynamics. For low levels of  $I$  ( $0 < I < 0.5$ ) the system has three fixed points (two stable, one unstable at  $u = v$ ). The speed of increase in  $y$  is faster the higher the input  $I$ . For intermediate values of  $I$  ( $0.5 < I < 1$ ) the system still shows three fixed points as in the low input regime (Fig. 2b), but  $y$  ramps up with a slope that is inversely proportional to the input  $I$  ( $y$  increases slower the higher input  $I$ , cf. Fig. 2c). For high  $I$  ( $1 < I$ ) the system has only one, but stable fixed point (at  $u = v$ ), and  $y$

decreases faster for higher  $I$ . Thus, the speed at which the output  $y$  evolves can be controlled by the input  $I$  (Fig. 2d) and determines the time interval after which  $y$  reaches a fixed threshold  $y_{th}$ . In interval reproduction experiments, reaching a threshold  $y_{th}$  can be understood as movement initiation time, which can be controlled for by adjusting  $I$ . In this section, the intermediate input regime is explored: higher inputs result in a shallower slope of  $y$ , such that the threshold  $y_{th}$  is reached after a longer time interval.

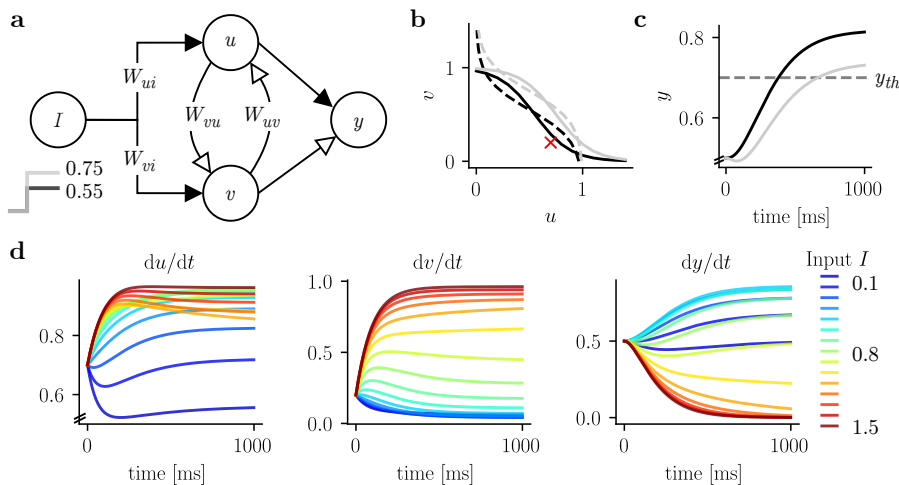


**Figure 2: Basic circuit and input regimes.** (a)  $u$  and  $v$  share a common input  $I$ . The input is governed by weights  $W_{uI}$  and  $W_{vI}$ . The two units have reciprocal inhibitory connections, with weights  $W_{uv}$  and  $W_{vu}$  that determine the inhibitory strength. Both project to the output unit  $y$  with an excitatory connection from  $u$  and an inhibitory connection from  $v$ . Excitatory and inhibitory connections are shown by filled and open arrows, respectively. (b) The control of the speed in  $y$  can be analyzed in the phase plane of  $u$  and  $v$ . The  $u$  (dashed) and  $v$  (solid) nullcline is shifted when the input is increased from  $I = 0.65$  (black) to  $I = 0.75$  (gray). In the intermediate regime, the system shows two stable and one unstable fixed point. The red cross indicates the initial conditions for the dynamics in (c). Depending on  $I$ , with the same initial conditions, the system evolves faster or slower to the stable fixed point. (c) Dynamics of  $y$  for intermediate regime with input  $I = 0.75$  in gray and  $I = 0.65$  in black. There is an inverse relation of input strength and slope. With higher input, the threshold at 0.7 (dashed line) is reached after a longer time interval. (d) Dynamics of  $u$ ,  $v$ ,  $y$  for inputs from  $0.1 \leq I \leq 1.5$  are shown. Initial conditions are set to  $u_0 = 0.7$ ,  $v_0 = 0.2$ ,  $y_0 = 0.5$ . With these initial conditions and values of  $I \geq 0.5$ , the relation of steady state activity of  $y$  (and slope to reach the steady state) is inverse to  $I$  (intermediate and high  $I$  regime). For values  $I \leq 1$  the activity of  $y$  ramps down (yellow corresponds to  $I = 1$ ). For  $I < 0.5$  the steady state (slope) is smaller the smaller  $I$  (low  $I$  regime, dark blue).

## 2.2 Extended Circuit for Experiment Simulation

Basic interval reproduction experiments can be designed with only two epochs: a measurement epoch that has the duration of the stimulus interval and a reproduction epoch that starts immediately after the measurement epoch (Fig. 3b).

Typically, a delay is introduced between subsequent trials. The basic circuit described above is modified to perform interval reproduction (cf. Figure 3a for schematic of the modified circuit). To achieve time reproduction, the relation of input  $I$  to the slope of the ramping activity of  $y$  is used in combination with a fixed threshold  $y_{\text{th}}$ . By introducing an update mechanism that flexibly adjusts  $I$ , the threshold crossing of  $y$  can be delayed or moved to an earlier time. This way, measuring and reproducing an interval is done predictively, by adjusting the slope of the ramp such that the output reaches the threshold after the intended time. In this model, the measurement epoch is specified by the stimulus interval  $t_s$ , whereas the reproduction ends when  $y$  reaches the fixed threshold  $y_{\text{th}}$  from below. The time from the end of the measurement epoch until the threshold-crossing of  $y$  yields the reproduced time interval  $t_r$ , which is aimed to equal the stimulus interval  $t_s$  (Fig. 3c).

**An update mechanism adjusts the input for reproductions.** In each measurement epoch, the external input  $I$  is inherited from the previous trial and needs to be adjusted for the subsequent reproduction. An error signal is determined from the difference of  $y$  to the threshold  $y_{\text{th}}$ . If the threshold  $y_{\text{th}}$  is not reached during the measurement epoch, the slope has to be adjusted, such that  $y$  ramps up faster to reach the threshold at exactly the time of the stimulus interval. For a steeper slope,  $I$  is reduced. If  $y$  crosses the threshold before the measurement epoch ends, and is therefore larger than  $y_{\text{th}}$  by the end of the stimulus interval, the slope needs to be reduced in order to reach the threshold at a later time in the reproduction. For a shallower slope,  $I$  is increased (Fig. 3c). The following update mechanism of  $I$  is based on the intermediate input regime, which shows an inverse relation of  $I$  to the slope of  $y$  (Fig. 2b).  $I$  is adjusted according to the error ( $y - y_{\text{th}}$ ), weighted by a memory parameter  $K$  right at the end of the measurement epoch

$$\tau \frac{dI}{dt} = sK(y - y_{\text{th}}) . \quad (2)$$

The update of  $I$  is only active for a pulse (one time step) between the measurement and reproduction epoch ( $s = 1$ ) and inactive for all other times ( $s = 0$ ). Moreover,  $u$  and  $v$  receive a transient input pulse  $I_r$  to reset the dynamics for the subsequent epoch (Fig. 3c)

$$\begin{aligned} \tau \frac{du}{dt} &= -u + \theta(W_{uI}I - W_{uv}v + \eta_u - I_r) , \\ \tau \frac{dv}{dt} &= -v + \theta(W_{vI}I - W_{vu}v + \eta_v + I_r) . \end{aligned} \quad (3)$$

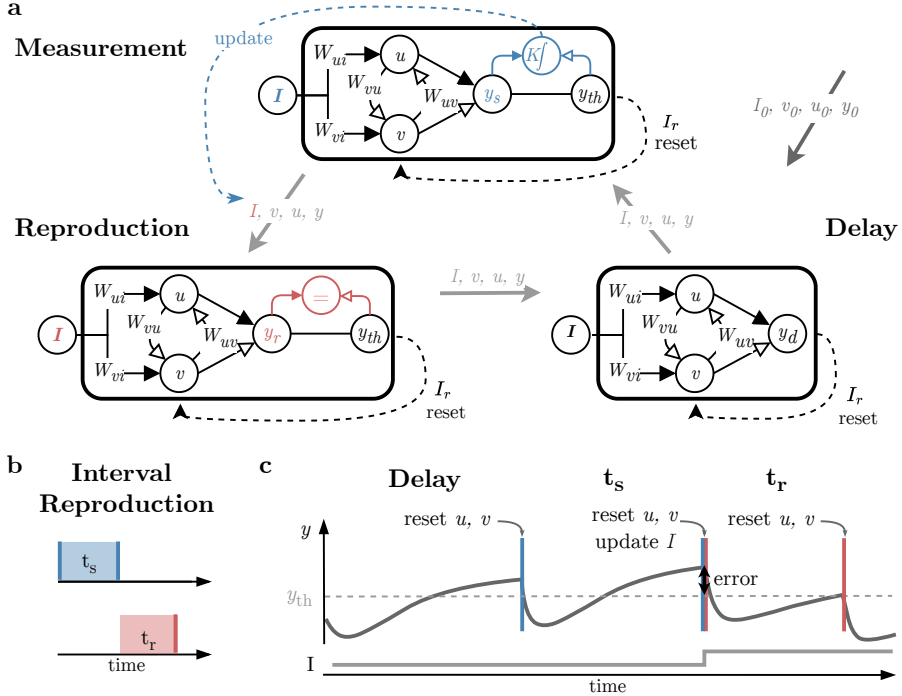


**Figure 3: Extended circuit for experiment simulation.** (a) The extended circuit comprises the circuits for measurement, reproduction, and delay epoch. All three circuits have the same underlying structure with different additional elements that are unique for the epoch. Initial values of  $u, v, y$  and  $I$  are fed into the delay circuit for the duration of the initial interval.  $u$  and  $v$  are reset with a transient input  $I_r$  before end values of  $u, v, y$  and  $I$  are transferred to the measurement circuit as new initial conditions. After the duration of the stimulus interval, the difference between  $y$  and the threshold  $y_{th}$  is used with the memory parameter  $K$  to update  $I$  together with another reset of  $u$  and  $v$ . The values are transferred with all other variables to the reproduction circuit. The reproduction epoch ends when  $y$  reaches the threshold  $y_{th}$  from below. Before the presentation of another stimulus interval, there is again a delay period with no update of  $I$ . The reset mechanism enables the model to simulate an arbitrary number of stimulus intervals. Adapted from Egger et al. 2020. (b) Interval reproduction experiment with stimulus interval  $t_s$  (blue) and reproduction  $t_r$  (red). (c) Schematic of one trial for interval reproduction. After a delay epoch,  $u$  and  $v$  are reset. The measurement epoch lasts for the duration of the stimulus interval  $t_s$ .  $y$  should reach the threshold  $y_{th}$  (dashed line) at exactly the time the stimulus interval ends. The threshold was crossed well before the end of the interval and at the end of the measurement epoch, the error in  $y_m$  to the threshold  $y_{th}$  is used to update  $I$ . To reach the threshold at a later time,  $I$  is increased, which reduces the slope of  $y$  in the reproduction epoch. After the reset of  $u$  and  $y$  and the update of  $I$  the reproduction ends when  $y$  reaches the threshold. The time after the reset and update until the threshold crossing denotes the reproduced interval  $t_r$ .

The reset mechanism is turned on for one time step after each epoch, allowing the model to reproduce any number of stimulus intervals in succession. Figure 4a depicts the activity of  $u, v, y$  and  $I$  in five example trials.

**Simulation of realistic time reproduction experiment.** In order to simulate a realistic time reproduction experiment, special attention had to be paid to the choice of stimuli and the noise level. In the full experiment simulation, a series of 500 trials was presented to the model. Stimuli were randomly chosen from a uniform distribution of time intervals that consisted of seven stimuli ranging from 400 to 700 ms, denoted as the stimulus range (Fig. 4b). To ensure that there were no side effects influencing the behavioral results, a repetition of all seven stimuli in a time window of 20 trials and no remarkable oscillation in the sequence of stimuli was required. In all simulations that were conducted in the intermediate regime, the threshold  $y_{\text{th}}$  was set to 0.7. The model worked with higher and lower thresholds robustly. To begin with, all three units had a time constant  $\tau = 100$  ms and initial conditions of  $u, v$  and  $y$  were set to  $u_0 = 0.7, v_0 = 0.2, y_0 = 0.5$ . Besides a fixed delay period of 700 ms between each trial, an initial interval at the beginning of the simulation was introduced which allowed the system to approach its steady-state before the first trial. The experiment simulation results in a distribution of inputs that drive the activity of  $y$  in the reproduction epoch and a distribution of reproduced time intervals for each stimulus (Fig. 4c).

To simulate variability in the reproductions, as it is present in real behavioral data, noise was added to  $u, v$  and  $y$  in the implementation as mentioned above. In behavioral data, a monotonic increase in the standard deviation of reproductions is found (*scalar variability*). The standard deviation of reproductions by the model grows monotonically for increasing stimulus intervals for all tested noise levels (Supplementary Fig. 1b). However, the increase in the standard deviation of reproductions plateaus with noise levels  $\sigma > 0.1$ . The coefficient of variation (CV) was used to quantify the degree of variation, defined as  $\text{CV} = \frac{\sigma_{\text{reproduction}}}{\mu}$  for each stimulus, where  $\mu$  corresponds to the stimulus interval and  $\sigma_{\text{reproduction}}$  to the standard deviation of the reproductions. To achieve variations close to real data, reproductions should have a CV of 0.1 to 0.4 that is constant over all stimulus intervals. For all simulations, the noise level  $\sigma$  was set to 0.02, for which the mean CV for the is 0.1 (Supplementary Fig. 1c).

**Classification of timeout trials.** Reproductions that did not reach the threshold in a certain time span or cross the threshold particularly early are classified as timeout trials. If the threshold was crossed before 20 % of the

stimulus interval has passed, the trial was categorized an early timeout trial. A late timeout was reported, when twice the stimulus interval had elapsed and the threshold had not been reached. Simulations that exceeded a fixed number of timeout trials (10% of all trials in the experiment) were excluded from analysis. If timeout trials occurred for a single stimulus more than 10% of all trials of this stimulus, the simulation was also discarded.

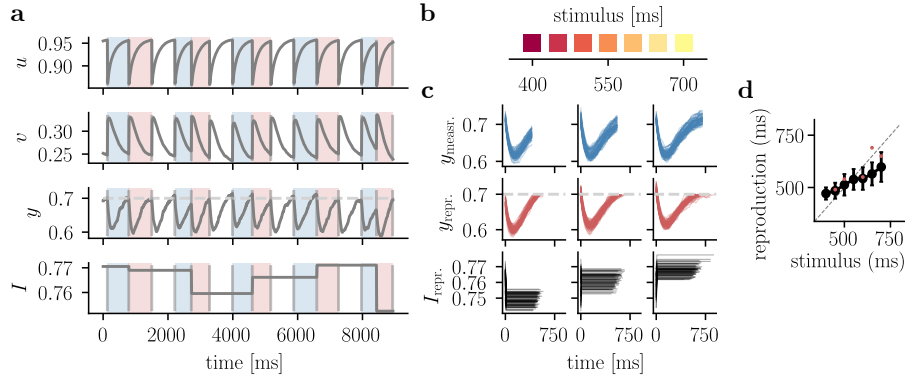


**Figure 4: Simulated reproduction experiment.** (a) The dynamics of  $u$ ,  $v$ ,  $y$  and  $I$  are displayed over time for five consecutive example trials (650, 500, 600, 700, 450 ms) of an experiment simulation with 500 trials total. Stimulus presentation and reproduction epochs are highlighted in blue and red, respectively. Before new stimuli presentations, there is a 700 ms delay period (white). Initial values for the experiment simulation are set to  $u_0 = 0.7$ ,  $v_0 = 0.2$ ,  $y_0 = 0.5$ ,  $I_0 = 0.8$ . The added noise is set to  $\sigma = 0.02$  and the memory parameter to  $K = 5$ . The threshold is set to  $y_{\text{th}} = 0.7$  (dashed line). Reproduced times are 690, 540, 550, 650, 490 ms. (b) For the experiment simulation, time intervals were randomly drawn from a discrete, uniform distribution. The range of time intervals contained stimuli from 400 to 700 ms, with steps of 50 ms. (c) The measurement (upper) and reproduction (middle) epoch of  $y$  and input for reproduction (lower) are shown for the full experiment, sorted according to stimulus interval. Shown are trials for stimuli of 400, 550 and 700 ms (depicted above). (d) Mean reproduction and standard deviation (black) across trials for each stimulus interval of the experiment stimulation shown (c). If the mean lies on the identity line (dashed line), reproduction time corresponds to the stimulus interval on average. Red dots show the reproductions of the example trials shown in (a).

Taken together, the model can be applied to simulate realistic time reproduction experiment with many consecutive trials. The noise level and weights were kept throughout the work. In contrast to Egger et al. (2020), initial values, especially  $I_0$ , did not need to be adjusted in advance. This is because the input has settled after the first one or two trials and is affected by the initial values thereafter. The mean over the distribution of reproduced time intervals for each stimulus allowed for the investigation of the behavioral results (Fig. 4d).

### 3 Model Parameters for Error Minimization

I asked whether the behavioral effects observed in real data (Fig. 1) could be reproduced by the circuit model. For this purpose, I focused on two model parameters,  $K$  and  $\tau$ , and adjusted them to minimize errors in the behavior. As mentioned above, other parameters like the noise level and initial conditions were always kept the same throughout experiments. The memory parameter  $K$ , was a crucial value to adapt, since it defines the weight with which the input is adjusted to compensate for the discrepancy between the predicted interval and the stimulus duration. The second parameter that I considered was the time constant  $\tau$ , which affects how fast the dynamics change in response to the input. Therefore,  $\tau$  can be interpreted as a biophysical parameter of the model that describes the rate of a population. To allow an investigation of the parameters decoupled from the influence of noise, I first used the same stimulus series and second initialized the added noise equally in each simulation. This way, I was able to extract changes in the behavioral results based on parameters only.

For evaluating behavioral characteristics like the range effect, two stimulus ranges were used in simulations, denoted as short and long range. The short range contained seven stimuli ranging from 400-700 ms. The long range consisted of the same number of stimuli, but these were shifted by 300 ms compared to the short range, resulting in a range from 700-1000 ms (Supplementary Fig. 1a).

#### 3.1 Behaviorally Plausible Time Reproductions

Before evaluating the behavior of the model, I introduce a more rigorous description of the behavioral effects. The regression effect in behavior can be quantified by the slope that results from a linear regression between the stimuli and the reproductions. Biologically plausible slopes are around 0.83 for the short and 0.73 for the long range (Sohn et al. 2019, Henke et al. 2021). To evaluate the model, the slopes of behavioral results were obtained for several combinations of the update parameter  $K$  and the time constant  $\tau$ . This resulted in broad parameter regimes in which reproductions show a regression to the mean, as indicated by a slope less than one. For fixed  $\tau$ , the regression increases as  $K$  increases, since more weight is given to the current update, and consequently less reliance is placed on the prior. The model exhibits biologically plausible slopes in the behavior for different time constants (Fig. 5a), where  $K$  must be adjusted depending on the stimulus range and time constant. To produce plausible slopes,  $K$  takes on smaller values for the long range, putting less weight on the update compared to the short range. This raises the question based on which criteria parameters should be chosen for the simulation.

**Mean squared error to determine model parameters.** To find suitable parameters independently of the slopes, I minimized the error of mean interval reproductions. The mean squared error (MSE) was defined as  $\text{MSE} = \text{bias}^2 + \text{var}$ , where the bias was expressed as the squared difference between the mean reproduction  $\bar{t}_r$  for each stimulus interval  $t_s$  and variance as mean  $\sigma^2$  for all stimulus intervals

$$\begin{aligned}\text{bias} &= \frac{1}{N} \sum_{i=1}^N (\bar{t}_{r_i} - t_{s_i}) , \\ \text{bias}^2 &= \frac{1}{N} \sum_{i=1}^N (\bar{t}_{r_i} - t_{s_i})^2 , \\ \text{var} &= \frac{1}{N} \sum_{i=1}^N (\sigma_i^2) .\end{aligned}\tag{4}$$

This error reflects the trade-off between bias and variance, with the bias error indicating over-assumptions (underfitting) and the variance indicating variability across reproduction and thus sensitivity to noise (overfitting).

### 3.2 Model Regime for Error-Minimized Behavior

Parameters that minimize errors in reproductions, are close to those that result in behaviorally plausible slopes. Furthermore, the effects observed in real data (Fig. 1) could be reproduced with these parameters.

For increasing time constants  $\tau$ , the optimized update parameter  $K$  increases as well. Values of  $K$  that minimize errors are smaller for the long range compared to the short range for all  $\tau$ , as already found for values of  $K$  that result in plausible slopes. The weight parameter that minimizes the MSE for each  $\tau$  is denoted as  $K^*$ . Across time constants,  $K^*$  is slightly lower compared to the weights that yield plausible slopes for the short range. In contrast, for the long range,  $K^*$  is slightly larger compared to weights that yield plausible slopes. Only for small  $\tau$  (below 120 ms),  $K^*$  drops to low values. Although the parameters do not directly coincide, weights that minimize errors are strikingly close to weights that yield plausible behavior (Fig. 5b).

The time constant that corresponds to the overall minimum of the MSE, denoted as  $\tau^*$ , differs between the two stimulus ranges: For the short stimulus range,  $\tau^* = 120$  ms and  $K^* = 11$  yield an overall minimum, whereas for the long range parameters are  $\tau^* = 200$  ms and  $K^* = 20$  (For behavioral results cf. Supplementary Fig. 2a, b). Assuming a constant  $\tau$  across experiments, I had to find a shared time constant for both the short and long range. Consequently, a time constant between the optima was chosen, considering the overlap with

biologically plausible slopes. With a time constant of 130 ms, optimal  $K$  matches with biologically plausible slopes for both ranges (Fig. 5b). Different noise initialization slightly influences the optimal value of  $K$ . For 20 simulations mean  $K^*$  and standard deviation for the short range are  $K = 12.88$ , std = 0.34 and  $K = 8.57$ , std = 0.99 for the long range.

**Behavioral results with error-minimizing parameters.** Behavioral results of simulations with error-minimizing parameters show a regression to the mean. The range effect is reflected by a stronger regression for the long range (slope of 0.73) compared to the short range (slope of 0.77) (Fig. 5c). Furthermore, the standard variation of reproductions increases linearly (*scalar variability*). The mean coefficient of variation (CV) for the short range is 0.09 and 0.11 for the long range (Fig. 5c). Summarizing, adjusting  $K$  in accordance with error minimization results in putting more weight on the prior experience for longer stimuli, which naturally entail more uncertainty, and is thus biologically plausible. Error-minimized parameter are close to parameters that yield plausible slopes, and key behavioral effects are reproduced. However, for all optimized values, there is a general underestimation of stimulus intervals for the long range, which becomes appeared in Supplementary Fig. 2e. The dynamics of  $y$  for single trials over the course of the experiment are shown in Supplementary Fig. 3.

**Parameters choice based on minimal bias and variance.** Next, I disentangled the MSE and investigated the contributions of variance and (squared) bias separately (Eq. 4). When error-minimization was based on the squared bias,  $\tau^*$  is smaller for both stimulus ranges. This means, the variance increases the optimal time constant. Similarly,  $K^*$  is decreased by the variance (Supplementary Fig. 2c, d). No range effect could be observed when minimizing the error in reproductions based on only the squared bias or only the variance. Moreover, the relation of stronger weighting of the prior for the long range due to decreased  $K$  is not apparent for either error metrics (Supplementary Fig. 2c, d). This is why I conclude that the MSE is a suitable choice to determine  $K$  and  $\tau$ .

### 3.3 High Input Regime

Even tough, there are differences between the intermediate and high input regime in terms of fixed points and dynamics, simulations of time reproduction experiments are possible in both regimes. One reason to look closer at the

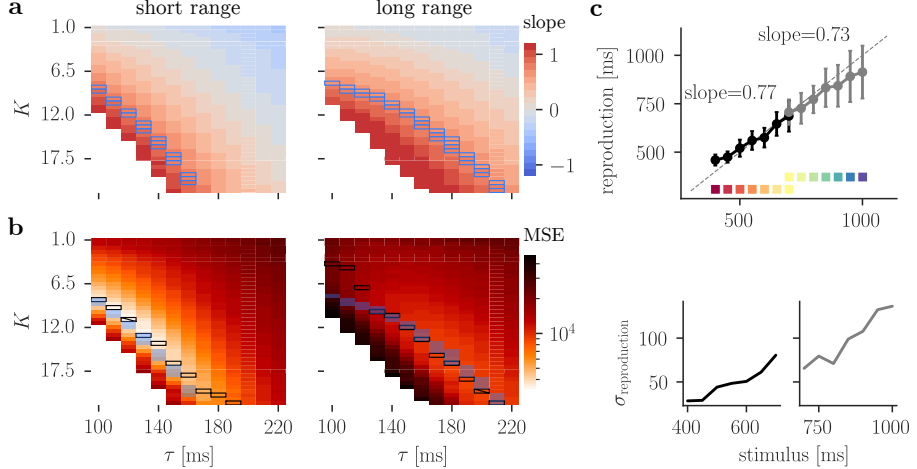


**Figure 5: Time reproductions with parameter that minimize errors.** (a) Simulations with 500 trials for each pair of memory parameter  $K$  and time constant  $\tau$  at noise level  $\sigma = 0.02$ . Simulations were performed with stimuli chosen from the short (left) or long range (right). Color scale represents the slope of the linear fit between stimuli and reproductions. A slope of 1 on the identity line corresponds to perfect reproduction of the stimuli. Behaviorally plausible slopes around 0.83 for the short and 0.73 for the long range are encircled in blue. Empty spaces correspond to simulations that exceeded the number of timeout trials and were thus excluded from analysis. (b) Optimization of the weight given to the update  $K$  for different time constants  $\tau$  at noise level  $\sigma = 0.02$ . Color scale represents the MSE for an experiment stimulation with 500 trials for each pair of  $K$  and  $\tau$ . Stimuli were either chosen from the short (left) or the long stimulus range. The minimal error for each  $\tau$  is encircled in black, and minimal error across all  $\tau$  is additionally crossed. Parameter combinations that result in behaviorally plausible slopes (a) are shaded in blue. (c) Top: Mean reproductions for simulation with 500 trials for each stimulation with the short (black) and long (gray) stimulus range. The value of  $K$  is optimized for a time constant of  $\tau = 130$  ms. Optimal  $K^*$  is 13 in the simulation with short stimulus range, and 10 with long stimulus range. The slope is the result of a linear regression between stimuli and reproductions. Inset: For experiment simulations, two stimulus ranges were used. The short range contained stimuli from 400 to 700 ms, the long range contained stimuli from 700 to 1000 ms. Bottom: Standard deviation of reproductions for each stimulus for the short and long range from the simulation in (c).

high input regime was, that the dynamics of  $y$  all converge towards the same steady state, whereas in the intermediate input regime, for different inputs,  $y$  evolves towards different steady states. In the following section, I investigate simulations in the high input regime and compare results with those in the intermediate input regime.

**Comparison of dynamics to the intermediate input regime.** While in the intermediate input regime three fixed points emerge in the phase plane (two stable and one unstable), in the high input regime the fixed points merge to a single one. The single fixed point is located at comparatively high activity of  $u$  and  $v$  (Fig. 6b, d). This affects the dynamics of  $u$  and  $v$  such that  $y$  decreases instead of increased as observed in the intermediate regime. Increasing  $I$  results in steeper activity of  $y$  in the high input regime. This is reversed compared to

the intermediate input regime, where an increased  $I$  leads to flatter slopes in  $y$  (Fig. 6a, c).

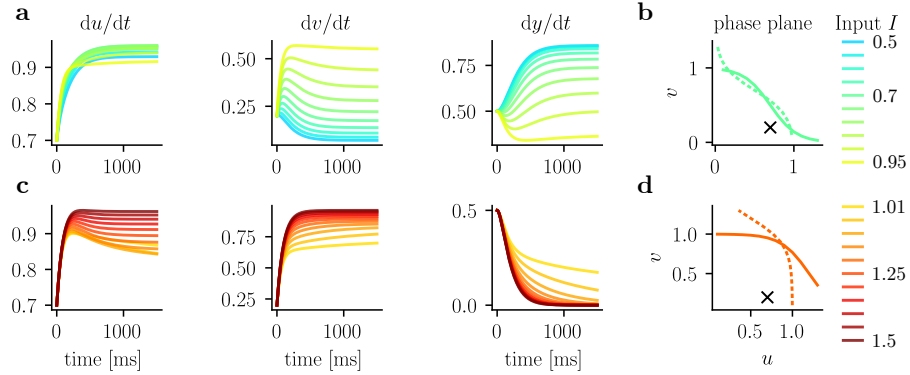


**Figure 6: Comparison of dynamics in the intermediate and high input regimes.** (a) Evolution of  $u$ ,  $v$  and  $y$  over time for different inputs (from 0.5 to 0.95) in the intermediate input regime. Activity in  $y$  shows an increasing activity. The activity of  $y$  evolves to different steady states depending on the input. (b) The phase plane in the intermediate input regime shows two stable and one unstable fixed point. The nullclines of  $u$  (dashed) and  $v$  (solid) are shifted to higher activities when the input  $I$  is increased. The plot shows nullclines corresponding to an input of 0.7, and the black marker indicates the initial condition of dynamics in (a). (c) Same as (a) for the high input regime with inputs from 1.01 to 1.5. Activity in  $y$  shows a decreasing activity, converging to 0 independent of input. (d) Same as (b) for high input regime. The phase plane in the high input regime shows one stable fixed point. The nullclines of  $u$  (dashed) and  $v$  (solid) are shifted to lower activities when the input  $I$  is increased. The plot shows nullclines corresponding to an input of 1.2 and the black marker indicates the initial condition of dynamics in (c).

**Experiment simulation and error-minimizing parameters.** To simulate time reproduction experiments in the high input regime, the following changes were made. The threshold was set to a value lower than 0 (e.g. 0.1) and initial  $I$  was increased to a value above 1 ( $I_0 = 1.02$ ). The reset impulse after each epoch had to be stronger by a factor of 10 and with opposite sign to bring the activity in  $y$  back to a higher level.

$$\begin{aligned} \tau \frac{du}{dt} &= -u + \theta(W_{uI}I - W_{uv}v + \eta_u + 10 * I_r) , \\ \tau \frac{dv}{dt} &= -v + \theta(W_{vI}I - W_{vu}u + \eta_v - 10 * I_r) . \end{aligned} \quad (5)$$

There was no need to change the update mechanism, even though the relation of the input  $I$  and the slope is reversed. This is because  $y$  approaches the threshold from above and not from below, so the relation of  $y$  and  $y_{\text{th}}$  is reversed and the update of  $I$  is correct.

The noise was set to the same value as in simulations in the intermediate regime ( $\sigma = 0.02$ ), which also lead to a linear increase in standard deviations. For increasing  $\sigma$ , the standard deviation drops slightly and then plateaus for  $\sigma$  larger than 0.1. The CV has similar values as in the intermediate regime, with 0.13 for the short and 0.12 for the long range for a  $\sigma$  of 0.02 (Supplementary Fig. 4a). An example of the experiment dynamics for four consecutive simuli is displayed in Fig. 7a.

Just as for the intermediate input regime, I identified parameters  $K^*$  and  $\tau^*$  that minimize the MSE of reproductions. Again, the model is capable to produce biologically plausible slopes for most time constants (Supplementary Fig. 4b). The weight  $K$  that minimized errors is smaller compared to the weights that yield plausible slopes for both ranges. For all  $\tau$  larger 40 ms, optimal  $K$  is smaller for the long range compared to the short range (Supplementary Fig. 4c). The MSE is minimal for  $\tau^* = 60$  ms for both the short and the long range, with  $K^* = 4$  and  $K^* = 2.5$  for the short and the long range, respectively. Behavioral results of experiment simulation with error-minimizing parameters show a regression to the mean. For the long range, the regression has a slope of 0.68 and for the short range, the slope is 0.74, hence a range effect is present. In contrast to the intermediate input regime, however, standard deviations of the reproductions do not grow linearly in the long range (Fig. 7b). Dynamics of  $y$  over the whole experiment are displayed in Supplementary Fig. 5.

**The high input regime provides no improvement over the intermediate input regime.** The common steady state in the high input regime was an intriguing feature. However, previous results have shown that the intermediate regime exhibits behavior closer to characteristic effects found in time estimation, e.g. monotonic increase in standard deviations of the reproductions. To compare one last property, I looked at the relation of the mean input in the reproduction epoch for each stimulus in an experiment. The mean input  $I$  shows an almost linear increase (or decrease for the high input regime) within a range. The increase (or decrease) is shallower for the long range due to the lower  $K^*$  used in the simulation (Fig. 8b, d). The maximum and minimum input  $I$  during the simulation for the short or the long range were used to examine the most distant nullclines of  $u$  and  $v$  in the phase plane (Fig. 8a, c). In the intermediate regime, the difference between maximal and minimal  $I$  is larger and the nullclines are also further apart. Other than that, no difference can be identified between the regimes. Taken together, the high input regime offers no improvement, if not a deterioration, over the intermediate regime. Therefore, I based

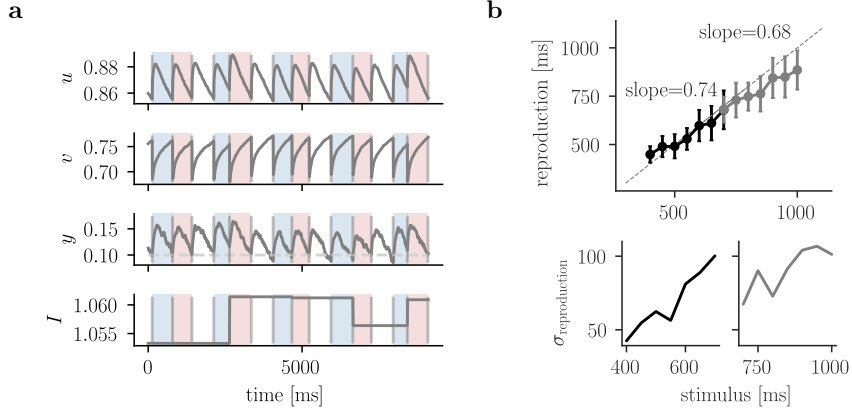


Figure 7: **Experiment simulation in the high input regime.** (a) Activity of  $u, v, y$  and  $I$  for five example stimulus intervals of 650, 500, 600, 700, 450 ms. Stimulus presentation and reproduction epochs are highlighted in blue and red, respectively. The delay period between trials is shown in white. Initial values are set to  $u_0 = 0.8, v_0 = 0.6, y_0 = 0.1, I_0 = 1.04$  and the threshold  $y_{th}$  is set to 0.1. (b) Top: Mean reproductions for simulation with 500 trials for each stimulation with the short (black) and long (gray) stimulus range. The value of  $K$  is optimized to minimize errors in reproductions for a time constant of  $\tau = 60$  ms. Optimal  $K^*$  is 4 for the simulation with the short range and 2.5 with long stimulus range. The slope is the result of a linear regression between stimuli and reproductions. Bottom: Standard deviation of reproductions for each stimulus for the short and long range from the simulation in (b).

the following analysis only on the intermediate regime.

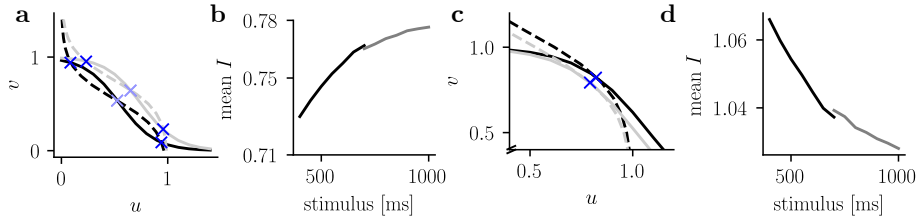


Figure 8: **Comparison of experiment simulations.** (a) The phase plane in the intermediate input regime shows two stable (blue) and one unstable (light blue) fixed points. The nullclines of  $u$  (dashed) and  $v$  (solid) are displayed. Black and gray nullclines correspond to an input of 0.71 and 0.79, respectively, which represents the maximal and minimal input in the experiment simulation for the short and long range in Fig. 5c. (b) Mean input during the reproduction epoch for each stimulus of the short (black) and long (gray) range for the experiment simulation in the intermediate input regime with optimized parameters from Fig. 5c. (c) The phase plane in the high input regime shows one stable (blue) fixed point. The nullclines of  $u$  (dashed) and  $v$  (solid) are displayed. Black and gray nullclines correspond to an input of 1.081 and 1.017, respectively, which represents the maximal and minimal input in the experiment simulation for both the short and long range in Fig. 7b. (d) Same as (b) for the experiment simulation in the high input regime with optimized parameters from Fig. 7b.

## 4 General Underestimation of Reproductions

The indifference point of the reproductions to the stimuli is shifted to lower values in the long range. However, because of the central tendency of reproductions, the indifference point of a linear regression between stimuli and reproductions should correspond to the mean of the stimulus range. This is the case for the short range, where the indifference point corresponds to 595 ms, which is close to the range's mean value of 550 ms. For the long range, the indifference point is 710 ms, and thus considerably smaller than the range's mean of 850 ms (for behavioral results, cf. Fig. 5c). This means that stimuli in the long range are generally underestimated.

What is the reason for the general underestimation of larger inputs (Fig. 11a)? Across time domains, it is not uncommon for stimuli in larger ranges to have lower estimates. Time reproduction experiments with gerbils, for example, show a general underestimation across ranges (Henke et al. 2022). The cause of this has not yet been studied and could be due to many reasons, ranging from lapsing attention to impatience. It is necessary to investigate whether the underestimation in the model's behavioral output is caused by the regime in which the model operates, or whether it is a phenomenon that arises from optimal choice of parameters. Possible parameters that could influence the behavior of the model are the delay period between trials, the fixed threshold and the common time constant between stimulus ranges.

### 4.1 Time Constant and Delay Influence Reproductions

Adjusting the time constant can counteract the general underestimation of reproductions. Simulations in the previous sections were performed with a common time constant  $\tau$  that was set between the optimal  $\tau^*$  for the short and long range, respectively. General underestimation in simulations with the long range can be compensated by increasing the time constant towards the optimum of the long range. However, this causes a general overestimation in the simulation with the short range (Supplementary Fig. 2b). Thus, a common time constant  $\tau$  contributes to the under- and overestimation of stimuli when it is located too far from the optimum of the range. However, even with optimal  $\tau$ , simulations show a slight general underestimation in the long range. Hence, general underestimation is caused by multiple factors.

**The delay between trials causes skewed reproductions.** For both the long and short range, the best reproductions are obtained for stimuli near 700 ms. Following this observation, I simulated an experiment with a stimulus range that was situated around 700 ms, ranging from 550 to 850 ms. The

mean of 700 ms corresponds to the maximum of the short range and the minimum of the long range, and also complies with the length of the fixed delay period between trials. In Fig. 9a the behavioral results show regression to the mean with a slope of 0.82 and an indifference point of 657 ms. When setting the delay period to the maximum of the long range instead (1000 ms), a general overestimation of stimuli from the short range occurs (Supplementary Fig. 6c). I therefore assumed that a delay period too far from the range's mean results in under- or overestimation. A comparatively short delay period compared to the mean of stimuli causes distorted updates because  $y$  cannot reach the threshold in the short time period with mean input strength  $I$ . After resetting, the following measurement period is started from lower values in  $y$ . Setting the delay period to be equal to the mean of the short or long range eradicates general underestimation (Supplementary Fig. 6a, b).

## 4.2 Adjusted Experiment Simulation

The previous analysis showed that there are two main problems causing distorted stimulus reproductions. First, a common time constant between experiments with different ranges skews the reproductions. Second, the experimental design should not bias reproductions, however the choice of the delay between trials interferes with correct reproductions.

Since the time constant in the model can be interpreted as a rate time constant, it is justifiable to adapt it between experiment with different stimulus ranges. This would correspond to a firing rate adjustment in the population to the experimental setting. In a biological system, an inhibitory population could scale the rate time constant according to the stimulus statistics.

**Omitting the delay period.** Furthermore, the model had to be adjusted to take into account the impact of the delay period on the reproductions. Setting the delay time to the mean of the stimulus range used in the simulation does not make sense from a design perspective. It should be possible to choose the delay period between trials arbitrarily and independently of the stimulus range. Similarly, the delay period could be set to be long enough to allow the system to evolve to a steady state. However, this would mean that the delay time cannot be chosen independently.

Another way to solve the problem of the delay epoch, was to neglect the delay in the simulation of the experiment (Fig. 9b). The reproduction period always ends when the threshold  $y_{\text{th}}$  is met. If the measurement period of the subsequent trial follows directly after it, it always starts at the same value of  $y$ . This does not necessarily mean that the experimental design is limited.

When simulating experiments that include a delay period between trials or even between measurement and reproduction epoch, it can be assumed that information is stored in the system until the beginning of the next epoch. In neural networks, it has been shown that the timing information in the state space can be held over a delay time (Bi and Zhou 2020). Neglecting the delay epoch in combination with independent  $\tau^*$  for each range leads to characteristic effects and biologically plausible slopes (Fig. 9c). Solutions that incorporate a delay period into the simulation itself would require model adjustments. Either the reset is changed from an impulse to a fixed reset value, or the input is updated separately during the delay epoch based on an error to always reach the threshold.

Unless otherwise specified, error-minimizing  $\tau^*$  and a delay of 0 ms were used for each stimulus range in following simulations. The regime of  $I$  remains similar to previous simulations with delay and common  $\tau$ . There is an overlap in  $I$ , and  $K$  is no longer comparable due to separate  $\tau$  between different ranges (Fig. 10b).

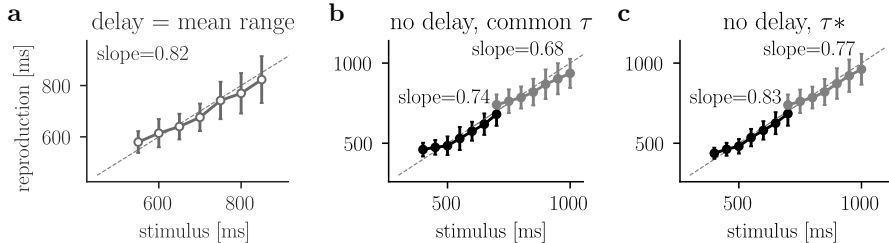


Figure 9: **Behavioral results with altered delay.** (a) Behavioral results of an experiment simulation with the previously utilized delay of 700 ms. The stimulus range that was used to sample stimuli from has a mean equal to the delay of 700 ms. The time constant and update parameter were both optimized based on the MSE ( $\tau = 170$  ms,  $K = 17.5$ ). Other parameters like threshold and initial values were not changed. (b) The delay period was set to 0 ms in simulations with the short and long range (black and gray, respectively). The time constant was set to 165 ms, which corresponds to the mean of the optimal  $\tau$  for the short (130 ms) and long (200 ms) range. For  $\tau = 165$  ms, the update parameter  $K$  was optimized (short range  $K = 21$ , long range  $K = 13$ ). Note different axes of figures in (a) and (b). (c) Same as (b) but with independent, optimal time constant. For the short range  $\tau^* = 130$ ,  $K = 14$  and for the long range  $\tau^* = 200$ ,  $K = 20$ .

## 5 Influence of External Variability on Behavior

Time reproductions are affected by internal noise and external variability of stimuli. Performance in time reproduction depends on the discrimination abilities of the individual subject. In the model, this is reflected by internal noise  $\sigma$ . But time reproductions not only depend on the current stimulus interval,

but also on context information and task-irrelevant influences (Bausenhardt et al. 2016). Variability of the environment is captured by the statistics of stimuli over the course of an experiment. When internal noise is fixed, the external variability can be modified independently. In this section, I examine the effects of external variability on behavior of the model, by changing the mean and the variance of stimuli separately. Comparing the behavioral results of the model with data from gerbils and humans, I found similarities and discrepancies that raise unresolved questions.

**Effects of stimulus statistics in real behavior** With larger time intervals, internal estimates get noisier and regression of reproductions gets stronger. This is well described by the *range effect* across species (Cicchini et al. 2012, Sohn et al. 2019), Henke et al. 2021, Henke et al. 2022. Besides the mean, the variance of stimuli can also influence reproduction. Larger variance can be achieved by reducing the sampling frequency of the stimulus range or by expanding the width of the range, accommodating more distant time intervals. The effect of changing the variance of stimuli on behavior has not been well studied. There are three different effects that greater variance could have on behavior. Reproductions could improve, leading to a weaker regression. This would mean that subjects rely less on the prior experience. Intuitively, larger variance means that differences in time intervals get more apparent and discrimination becomes easier (e.g. stimuli are further apart or extremes are more distinct). This scenario is predicted by a model that uses noisy integrators linked by an adaptive reference in Thurley (2016).

On the other hand, a change in variance might have no effect on behavior if the mean is fixed. According to this, only the mean value would have an influence on the reproduction performance. This seems to be the case in Petzschner et al. (2012), since performance of the range with larger variance does not improve. Finally, reproductions may worsen with greater variance. This was demonstrated in the case of sound intensity estimations by Teghtsoonian and Teghtsoonian (1978). In most studies that included experimental data with varying variance of stimuli, the effects on regression were not examined.

## 5.1 Optimality Predicts Key Effects

To test the behavior of the model with respect to the external variability of stimuli, additional ranges were introduced, which differed in mean, width, and sampling frequency. The short and the long range included seven stimuli spanning 300 ms, with mean values of 550 and 850 ms, respectively. Two ranges had the same variance and width, but shifted mean values at 700 ms (mid range)

and 1050 ms (extra-long range). With increasing mean, the range effect predicts a flatter slope. In addition, ranges with mean equal to the ranges above, but with higher variance were examined. Including all stimuli from the short and the long range, the all range had the same mean as the mid range, but a larger width (600 ms) and therefore higher variance. The short-few and all-few range encompassed the short and the all range, respectively, but with a smaller number of stimuli, the variance increases in both cases (Fig. 10a, Supplementary Fig. 7c).

For all ranges, the slope of the linear regression between stimuli and reproductions is below one. Thus, simulations with error-minimizing parameters predict the regression effect across several ranges. The slopes decrease significantly as the mean of the stimulus range increases, except for the short and mid range (Fig. 10c). Thus, the model predicts the range effect only for sufficiently large changes in the mean. (Kolmogorov-Smirnov two-sample test,  $p < 0.01$ ,  $n = 21$  for each distribution, Bonferroni correction for multiple testing). Across ranges that only change their mean value (short, mid, long and extra-long), the slope has a linear correlation with the mean value of the range (Pearson correlation  $r = -0.95$ ,  $p < 0.05$ ).

When the experiment was simulated with a common  $\tau$  of 165 ms between ranges,  $K^*$  is significantly lower for the mid range (16.71) compared to the short range (21.33), but slopes show no significant difference (Supplementary Fig. 7a, b). Decreasing  $K^*$  for increasing mean of ranges is captured by the model beyond the short and the long range. (Kolmogorov-Smirnov two-sample test,  $n = 20$  for each distribution,  $p < 0.01$ , Bonferroni correction for multiple testing).

**What causes the range effect in the circuit model?** The model is situated in a dynamic regime that displays time reproductions close to real behavior. Error-minimizing parameters predict the regression and range effect across multiple stimulus ranges. Decreasing slopes for larger stimulus ranges occur because they approach the limit of the dynamic regime (Fig. 10b). When the stimulus ranges are pushed to more extreme values, the behavior of the model breaks down. This breakdown is caused by too many timeouts, which occur when time intervals are too short. If time intervals are too long, the variance in reproductions increases sharply and  $K$  is pushed to lower values, resulting in slopes that are well outside the observed behavior. This means that the regime of the model has to be adapted to major changes in the external statistics.

## 5.2 Optimality Predicts no Effect of Variance on Behavior

How does the slope change when the mean of stimuli remains constant, but variance is increased? The statistics of stimuli can be summarized by the ratio of the mean and variance of the stimulus range:  $\frac{E(t)}{\text{Var}(t)}$ . Higher variance in ranges with lower stimulus sampling (short-few, all-few) shows no significant difference from their counterparts with normal stimulus sampling (short, all). Furthermore, a larger width of stimuli does not result in a significant larger or smaller slope (all range vs. mid range). Therefore, increasing variance is not affecting the reproduction of stimuli in the model (Kolmogorov-Smirnov two-sample test,  $n = 21$  for each distribution, Bonferroni correction for multiple testing). Considering only the mean, there is a significant correlation with the slope (Pearson correlation  $r = -0.96$ ,  $p < 0.001$ ), but not with the external variability ratio (Pearson correlation  $r = -0.65$ ,  $p = 0.12$ ) (Fig. 10c). In the simulation with a common  $\tau$ , there is no significant difference in  $K^*$  when the variance is changed (Supplementary Fig. 7a, b). However, increasing the variance of the range leads to a significant increase in MSE in all cases (Fig. 10d). (Kolmogorov-Smirnov two-sample test,  $n = 21$  for each distribution,  $p < 0.01$ , Bonferroni correction for multiple testing).

## 5.3 Comparison of Model Output to Real Data

The circuit model predicts that a change in variance affects the MSE of the reproductions. It also predicts that only the mean, but not the variance has an effect on the regression of reproductions, which is in contrast to the noisy integrator model proposed by Thurley (2016). In the following section, I compare predictions of the model with behavioral data from time reproduction experiments with gerbils and humans. The stimuli in these experiments were several seconds long and came from either a short, mid, long, or all range (data by Henke and Thurley, Henke et al. 2022).

**Time reproduction experiments with gerbils and humans.** Gerbils were trained to reproduce time intervals of a few seconds. The experiments were conducted with one stimulus presentation, the reproduction directly after and a delay period between trials (Henke et al. 2022). Behavior in gerbils exhibits a regression effect for all ranges and a range effect for ranges with increasing mean. The variation in slopes between gerbils is considerably larger when the variance is increased. At the individual level, both consistent and increasing performance with increasing variance is observed. There are three

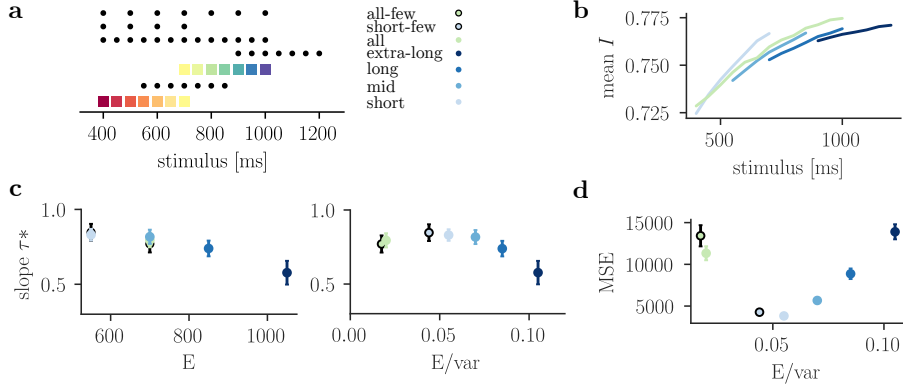


**Figure 10: Behavioral slopes with varying stimulus statistics.** (a) Parameter simulations were performed with stimulus ranges that differed in mean and variance to the short and long range. The mid range has its mean at the overlap of the short and long range. The extra-long range has its mean above the long range. Both the mid and extra-long range contain seven stimuli, just as the long and short range. To change the variance, a range with 13 stimuli that span the short and long range was included (all range). Both the short and the all range were for the short-few and all-few range undersampled. (b) Simulations were performed with optimized  $\tau^*$  (and corresponding  $K^*$ ): short 130 ms (14), mid 170 ms (17), long 200 ms (20), extra-long 230 ms (18), all 150 ms (14). Mean input  $I$  for each stimulus was calculated for stimulation with different ranges. Colors correspond to legend in (a). (c) Left: Slopes of behavioral results plotted against the mean of the range that was used. The error bars indicate standard deviation in the slope for different initialization. Colors correspond to legend in (a). Right: Slopes plotted against the ratio of the mean and the variance of each range. (d) The MSE for simulations with error-minimizing parameters plotted against the ratio of mean and variance of the range.

gerbils that show a linear increase in performance with decreasing ratio of the mean and variance of the stimulus range (Fig. 11b). The remaining four gerbils, however, show no effect of variance on reproductions (Supplementary Fig. 8a). On average, Pearson correlation reveals a significant linear relation of the slope with the mean ( $r = -0.62$ ,  $p < 0.001$ ) and ratio of mean and variance ( $r = -0.61$ ,  $p < 0.001$ ) in gerbils. This correlation gets stronger when the all range is excluded ( $r = -0.75$ ,  $p < 0.001$ ). Humans performed time reproduction with similar time intervals. Behavior is heterogeneous, only some individuals show a range effect (Fig. 11). There are no significant correlations of the slope with the mean or external variability ratio. The root MSE increases as the variance increases across all subjects (Supplementary Fig. 8b).

**The model captures only parts of the observed behavior.** The circuit model predicts no effect of variance on the regression, but only on the error in reproductions. Gerbils show a discrepancy in performance when variance is increased. The model captures only one observed behavior, not taking into account the information from a change in variance. Even though there is no correlation of the slope with the external variability ratio in the model, experiments in gerbils show that there is indeed a significant correlation ( $r=-0.61$ ,  $p < 0.001$ ).

However, the model correctly captures an increasing error in reproductions with higher variance (Fig. 10b).

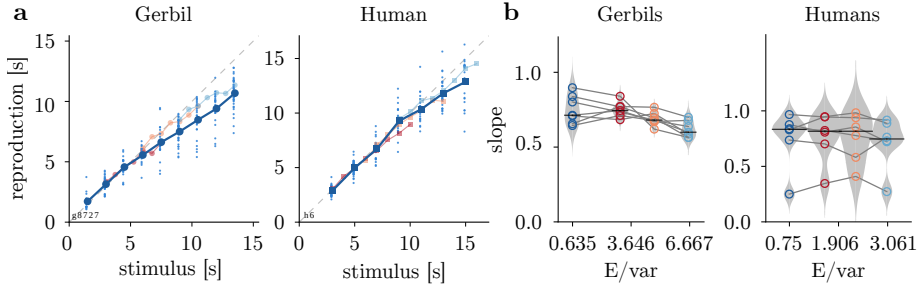


**Figure 11: Effects of stimuli statistics on behavior of gerbils and humans.** (a) Representative behavioral results of time reproduction of a gerbil (left) and a human (right). Stimuli were several seconds long. Four experiments were conducted with different ranges: short (red), mid (orange), long (light blue) and all (blue). Large markers display the mean of trials. Small dots show reproductions of single trials for the experiment with the all range. (b) Slope of the linear regression between stimuli and reproductions for seven gerbils (left) and six humans (right) plotted against the ratio of the mean and variance of the stimulus ranges. Vertical black markers indicate the median of slopes, and gray violin plots illustrate the distribution over all animals. Slopes for different stimulus ranges of one animal are connected by lines. Figure courtesy of Kay Thurley and Josephine Henke.

## 6 Discussion

Previous results indicated that time is encoded in dynamical changes of population activity, the rate of which is adjusted to the expected timing of movement initiation (Remington et al. 2018, Wang et al. 2018, Egger et al. 2019, Henke et al. 2021). This led to the hypothesis that control over timed behavior can be understood in terms of adjustments to initial conditions and external inputs of a dynamical system (Remington et al. 2018, Wang et al. 2018, Tsao et al. 2022). Further support was provided by the study of recurrent neural networks (RNNs) that were trained on time reproduction tasks. When trained with a tonic input, RNNs generated smooth temporal scaling when exposed to novel inputs. This was not the case for RNNs trained on transient inputs, supporting the hypothesis of the speed-control mechanism via a tonic input (Remington et al. 2018, Bi and Zhou 2020, Zhou et al. 2022). The circuit model takes the core of this mechanism, i.e. a dynamical systems approach, and combines it with other observations from data, like action triggering states or error signals, to facilitate time reproduction.

**Elements of the circuit model and their counterpart in real data.** Speed control is implemented via a tonic input to two neurons, such that the readout unit scales its activity with the input and reaches a fixed threshold at different times, corresponding to the triggering of a response. The threshold corresponds to the action-triggering state in the population activity, when the neural trajectory is projected onto the time axis (Remington et al. 2018). In each trial, the model updates the input according to the stimulus interval. Previous work showed that the population dynamics are sequentially updated based on an error signal to yield better estimates (Egger et al. 2019). In the model, the error signal is extracted from the distance of the magnitude of activity to the threshold in the measurement epoch. The error is combined with a weight and used to either increase or decrease the input to match the time of threshold crossing to the stimulus interval in the reproduction. For judgments about time, the brain is thought to rely on an internal reference that is sequentially updated over trials (Dyjas et al. 2012, Bausenhart et al. 2014). This concept is tightly connected to a Bayesian framework of magnitude estimation, where a prior is combined with current estimates (Shi et al. 2013, Petzschner et al. 2015). In the circuit model, the input level in the measurement is inherited from the previous trial and updated before the reproduction epoch based on the weighted error. Thus, the inherited input to the measurement epoch is composed of the initial input and all past updates, which can be interpreted as a moving average of preceding inputs. The mean input over the course of an entire experiment

reflects the prior or internal reference in the circuit model, corresponding to the mean stimulus interval.

However, Egger et al. (2019) showed in an experiment with two successive stimulus presentations that neural trajectories did not encompass a stimulus representation in the first measurement epoch but reflected the prior. In the second measurement epoch, the trajectory was adjusted, by updating a speed command based on an error. The speed with which the trajectory evolved was predictive of the reproduction. The error in the second measurement epoch was again used to update the speed command, which lead to a smaller bias in the trajectories in the reproduction epoch. The speed of neural trajectories therefore reflected a predictive process and sequential updating mechanisms initiated by a speed that reflects the prior.

To better approximate the prior or internal reference hypothesis in the stimulus presentation in the model, the input to each measurement epoch should be set to a value equal to the moving average of the previous inputs, rather than being inherited from the previous trial. Taken together, the model uses the core elements that have been observed in data, but in a simplified way, making it possible to study the resulting dynamics in depth. It has already been shown that the model captures the classical effects of magnitude estimation when fitted to human data (Egger et al. 2020).

Here, I extended the model to simulations of realistic time reproduction experiments that reflect stimulus variability by presenting random time intervals drawn from a stimulus distribution.

## 6.1 Representation of Stimulus Statistics

Simulations across a variety of stimulus ranges confirmed that the model captures classical behavioral effects in realistic experiment settings under a parameter regime that minimizes errors in reproductions. This suggests that adjusting neural dynamics based on an internal reference in the presence of noise could lead to the key effects found in time reproduction experiments, such as the regression effect, the range effect and scalar variability. Sohn et al. (2019) suggested that optimal integration of prior beliefs arise from the curved nature of neural trajectories. Based on the results from the circuit model, curvature of manifolds would not be necessary to achieve biases in the reproduction, as they result from a sequential weighted update of the speed command (external input), where the weight is adjusted based on the stimulus statistics.

Since the key effects of time estimation were reproduced in simulations, I tested additional parameters in the stimulus statistics, e.g. by modifying the variance of the stimulus distribution, to test the model’s behavior for different

external variability. Only few studies have investigated an internal representation of temporal statistics. Acerbi et al. (2012) showed that humans are capable to represent the statistics of stimulus distributions to their third moment in reproductions. However, the model did not predict an impact of the change in external variability on the regression effect, but did predict an impact on the error in reproductions. This finding was partially confirmed in gerbil data, although some animals differed from the group by accounting for the change in variance, as evidenced by an increase in performance of interval reproductions. Animals that considered the variance in the data seem to have adapted to the new stimulus statistics in contrast to the other animals. How neural dynamics adjusted to accommodate the new information provided by changed variance is still to be determined. Meirhaeghe et al. (2021) examined the adaptation to simultaneous changes in variance and mean of stimuli and identified modulations in the firing rates and adjusted speed in the population dynamic to take into account the new distribution mean. The influence of variance, however, was not investigated separately. Understanding how external stimulus statistics feed into the computations of timing in the brain can help us to identify the underlying mechanism. Further experiments should be conducted to investigate this shift to considering information from altered stimulus statistic. A gradual change in variance could reveal the difference between the animals' behavior in terms of adaptation to stimulus statistics. Animals that did not increase performance in the present data might do so if the variance is further increased. Based on new evidence, the model would need to be extended to account for this adaptation in dynamics that improves performance.

## 6.2 Scales of Timing

Timing encompasses various scales, ranging from milliseconds and seconds to circadian rhythms. This raises the question of how timing mechanisms can accommodate time computations for widely spaced intervals. Circadian rhythms are daily cyclic variations in behavior such as sleep and awake states that arise from gene expression cycles (Patke et al. 2020). Behavior on these timescales is not based on neuronal mechanisms, and circadian rhythms do not operate on the second or millisecond scale. While circadian rhythms clearly rely on distinct mechanisms to encode time, it is not obvious whether there are different timing mechanisms between subsecond and suprasecond scales(Buonomano and Karmarkar 2002, Buonomano 2007, Paton and Buonomano 2018, Tsao et al. 2022). Neural trajectories encoding time have been identified in both the subsecond (Sohn et al. 2019, Meirhaeghe et al. 2021) and suprasecond scale (Henke et al. 2021), though adaptations of dynamics seem to occur. This becomes ap-

parent when comparing the regression effect between experiments conducted with ranges in different timescales. The range effect does not propagate from the subsecond scale to ranges in the suprasecond scale. In other words, the slopes for regression are independent and start close to 1 for short ranges in the suprasecond scale.

Simulations with the circuit model revealed that there is a limited regime in which the model exhibits the classical magnitude estimation effects. For stimulus ranges that are much larger or smaller than those I used, the behavior of the model breaks down. This means that when the model is used in experiments with even shorter or longer time intervals, the operating regime of the model must be adjusted to accommodate for the new timescale. To return to the model implementation: No statement is made about the timescale. Rather, the scale is set arbitrarily from the outside by assigning a unit to the time bins. Thus, the model’s operating regime can be moved to other timescales by rescaling the time axis, which is equivalent to changing the units of time bins.

How the adaptation to different timescales is realized in terms of neural trajectories is unknown. A different form of adaptation of neural trajectories to experiment setting has been shown by Remington et al. (2018). In experiments that involved a gain in reproductions, they identified a flexible displacement of neural trajectories in the state space. Further experiments need to investigate if a displacement of neural trajectories could explain an adaptation to new timescales. It must be clarified whether this adaptation to the timescale is gradual or immediate. Future work on the model will need to identify how to incorporate this adaptation to timescales into the model, rather than imposing it externally.

### 6.3 Integration into Classical and Bayesian Framework

Classical models of timing can be categorized into two main classes. Dedicated models rely on specialized and centralized mechanisms, including oscillator models and pacemaker-accumulator models, that produce ramping activity in single cells. Intrinsic models, on the other hand, are based on local and general properties of neural circuits, comprising ramping models and state-dependent network models (Goel and Buonomano 2014, Paton and Buonomano 2018). A link between the circuit model and the main classes of timing models has already been made in Egger et al. (2020). The circuit model clearly belongs to the class of intrinsic models because it relies on the population dynamics that are ubiquitous in the brain. It is important to point out that this model does not depend on an internal pacemaker to track time, since time is encoded in changes of neural dynamics. Nevertheless, the model distinguishes itself from classical timing

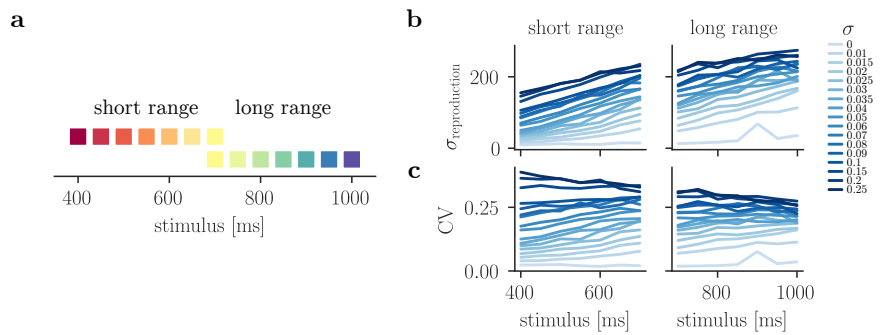
models because it is situated on a mechanistic level. It produces ramping activity through interactions of neurons, and allows for flexible behavior by adjusting to sensory feedback (Egger et al. 2020). This makes the model potentially useful for various behavioral tasks. In addition, the model is based on a circuit that is classically used for decision making.

**Link to the Bayesian framework.** A statistical approach that is often used to explain effects in timing behavior is the Bayesian framework (Petzschner et al. 2012, Shi et al. 2013, Petzschner et al. 2015, Sohn et al. 2019). While perceptual systems might be Bayesian at the computational level, they are probably not at the algorithmic and implementation level (Marr and Poggio 1977, Block 2018, Kwisthout and Rooij 2020). The circuit model is situated at the algorithmic level, possibly providing an algorithmic implementation of the Bayesian framework. The input to the model in the measurement epoch represents prior information about previous trials. Based on this prior information, the simulation period yields an error signal that is dependent on the current stimulus interval. With a weighted update of the input, prior information is combined with current sensory information, to accomplish correct estimates. The weight depends on the external variability, i.e. length of time intervals.

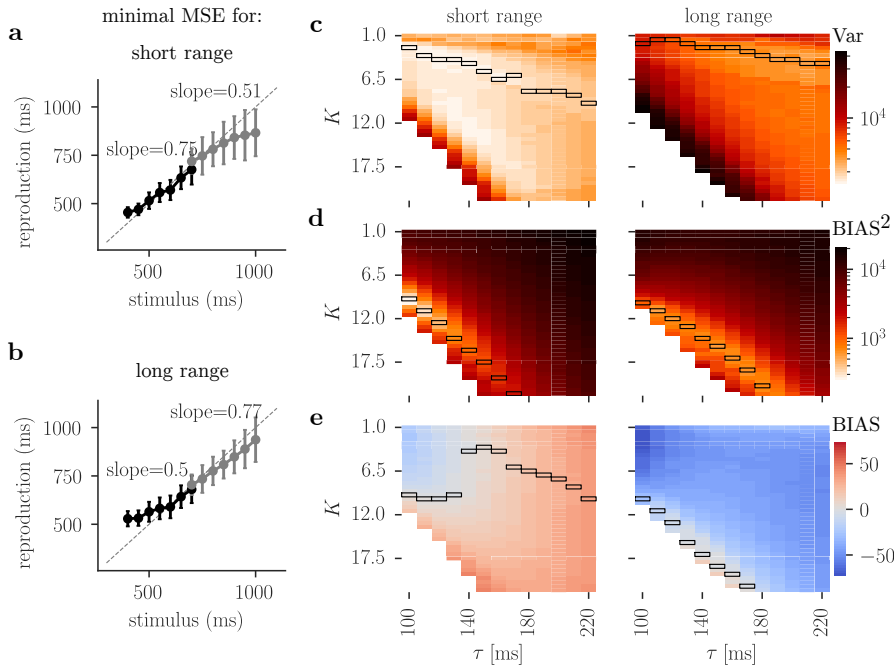
The circuit model is able to link neural activity to behavior and explains the key effects of magnitude estimation by combining prior information with a weighted error signal. Certainly, there are more factors, such as non-temporal context, e.g. intensity effects or sensory modality differences, that are not captured by the model. This work, however, provides further evidence that a dynamical systems perspective has the potential to explain flexible timing.

## Supplements

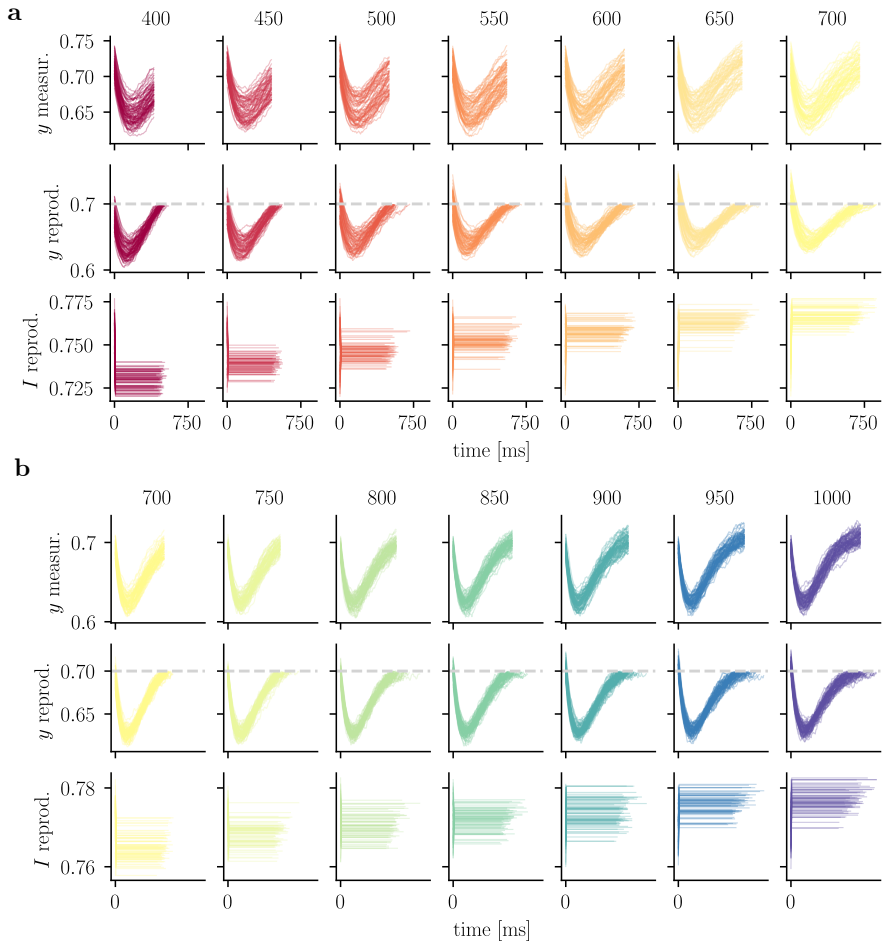
### Supplementary Figures



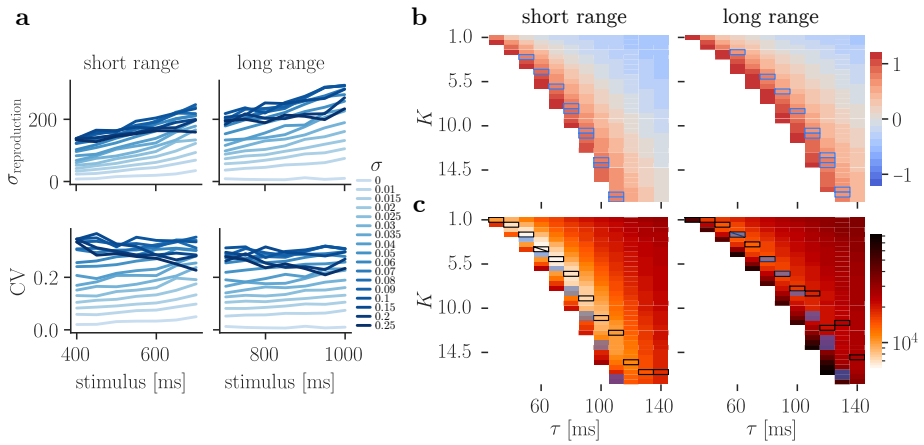
Supplementary Figure 1: **Experiment description and noise levels.** (a) The short and the long stimulus range comprised time intervals from 400 to 700 ms and 700 to 1000 ms, respectively. (b) Standard deviation of reproductions for each stimulus in an experiment simulation with 500 trials and  $\tau = 100$ .  $K$  was set to 8.5 and 6 for the short and long range respectively. (c) Same as (a), but the standard deviation of reproductions was normalized by stimulus duration (CV). For a noise level of  $\sigma = 0.02$ , the mean CV was 0.1 for the short range and 0.15 for the long range.



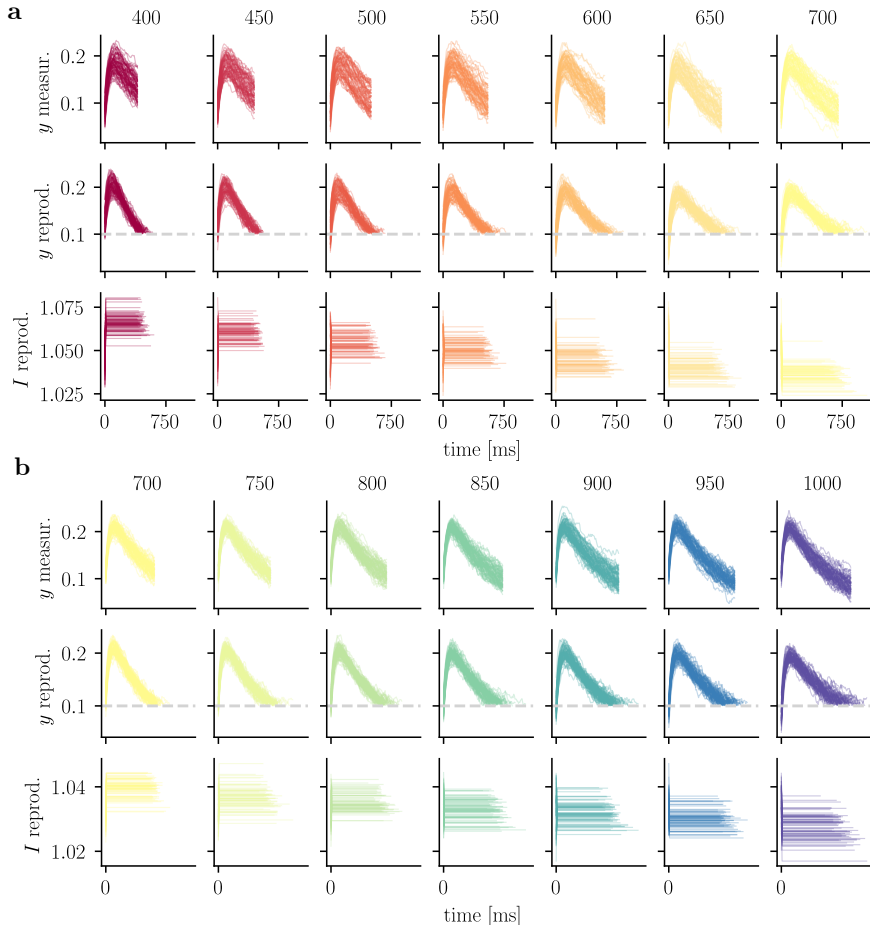
Supplementary Figure 2: **Extended parameter optimization.** (a) Behavioral results for a simulation with 500 trials,  $\sigma = 0.02$  and optimized time constant  $\tau$  for the short range ( $\tau = 120$ ). For simulations with both short and long range, the optimal time constant for the short range was used. Optimal  $K^*$  for  $\tau = 120$  was 11 for the short and 7 for the long range. (b) Same as (a) with optimized  $\tau$  for the long range ( $\tau = 200$ ). Optimal  $K$  for this time constant was 25 for the short range and 20 for the long range. (c) Simulations with 500 trials for each pair of memory parameter  $K$  and  $\tau$  at noise level  $\sigma = 0.02$ . Simulations were performed with stimuli chosen from the short (left) or long range (right). Color scale represents the variance of reproductions in the behavioral results. Minimal variance for each  $\tau$  is encircled. (d) Same as (c), color scale represents the squared bias of reproductions. Minimal squared bias for each  $\tau$  is encircled. (e) Same as (d); color scale represents the bias of reproductions. Values larger than 0 correspond to an overestimation, values smaller than 0 to an underestimation of the stimulus interval. Bias closest to 0 for each  $\tau$  is encircled.



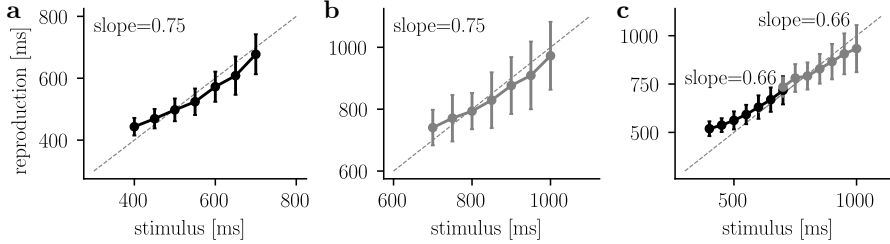
Supplementary Figure 3: **Experiment dynamics with optimized  $K$ .** (a) For an experiment simulation with 500 trials, a time constant  $\tau$  of 130 and optimal  $K = 13$ , the activity was sorted according to epoch and stimulus interval. Stimuli were chosen from the short range. The upper row shows the behavior of  $y$  in the measurement epoch and the middle row shows the behavior of  $y$  in the reproduction epoch. The lower row shows the input level to the circuit during the reproduction epoch. (b) Same as (a) with stimuli chosen from the long range and  $K = 10$ .



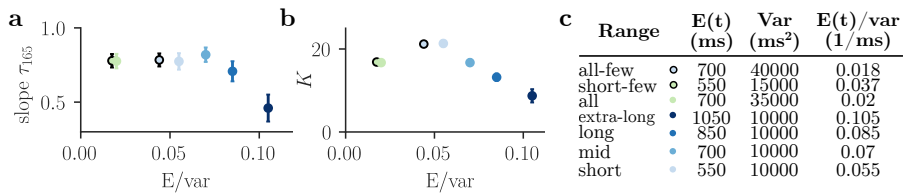
Supplementary Figure 4: **Experiment description and parameter optimization in the high input regime.** (a) Evaluation of noise for the high input regime of the model. Standard deviation (upper) and CV (lower) of reproductions for each stimulus in an experiment simulation with 500 trials and  $\tau = 70$ .  $K$  was set to 6 and 4 for the short and long range, respectively. (b) Simulations with 500 trials for each pair of memory parameter  $K$  and time constant  $\tau$  at noise level  $\sigma = 0.02$ . Simulations were performed with stimuli chosen from the short (left) or long range (right). Color scale represents the slope of the linear fit between stimuli and reproductions. Behaviorally plausible slopes are encircled in blue and lie around 0.83 for the short and 0.73 for the long range. Empty spaces show simulations that exceeded the number of timeout trials and were thus excluded from the analysis. (c) Optimization of the memory parameter  $K$  in the high input regime for different time constants  $\tau$  at noise level  $\sigma = 0.02$ . Color scale represents the MSE for an experiment stimulation with 500 trials for each pair of  $K$  and  $\tau$ . Stimuli were either chosen from the short (left) or the long stimulus range. The minimal error for each  $\tau$  is encircled in black, and minimal error across all  $\tau$  is crossed. Parameter combinations that result in behaviorally plausible slopes (b) are shaded in blue.



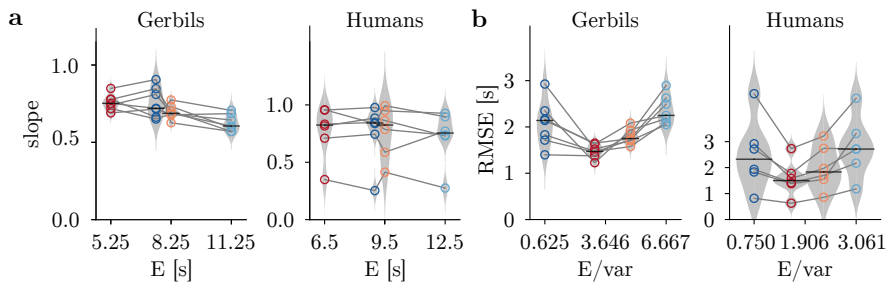
Supplementary Figure 5: **Experiment dynamics in the high input regime.** (a) For an experiment simulation with 500 trials in the high input regime, the threshold was set to  $y_{\text{th}} = 0.1$  and  $\sigma = 0.02$ . Parameters are set to optimized values with time constant  $\tau = 60$  ms and  $K = 4$ . The activity was sorted according to epoch and stimulus interval. Stimuli were chosen from the short range. The upper row shows the behavior of  $y$  in the measurement epoch, while the middle row displays the behavior of  $y$  in the reproduction epoch. The lower row shows the input level to the circuit during the reproduction epoch. (b) Same as (a) with stimuli chosen from the long range and  $K = 2.5$ .



Supplementary Figure 6: **Behavioral results with different delay periods.** **(a)** Behavioral results of an experiment simulation with stimuli of the short range and the delay period set to the mean of short range (550 ms). Time constant and update parameter were optimized by minimizing the MSE ( $\tau = 130$ ,  $K = 13$ ). Other parameters like  $\sigma$ , threshold and initial values were not changed compared to previous simulations. **(b)** Same as (a) but for the long range with the delay period set to mean of the long range (850 ms). Optimized  $\tau = 220$  and  $K = 22$ . **(c)** Behavioral results of experiment simulation with both the long and the short range and the delay period set to 1000 ms. The time constant was set 160 ms, which corresponds to the mean of the optimal  $\tau$  for the short (110 ms) and long (210 ms) range. Optimal  $K$  for the short ( $K = 17$ ) and long ( $K = 11$ ) range is optimized for the chosen time constant.



Supplementary Figure 7: **Influence of external variability on behavior with shared time constant.** **(a)** The slope of behavior resulting from experiment simulations with optimized  $K$  for different ranges was determined and plotted against the ratio of mean and variance of the stimulus range. The time constant was set to 165 ms for all ranges, which corresponds to the mean of the optimal time constant of the short and long range. The error bars indicate standard deviation in the slope for different initializations. Colors correspond to the legend in (c). **(b)** Values of  $K$  that minimized errors for a time constant of 165 ms for all ranges are plotted against the ratio mean and the variance of the stimulus range. The error bars indicate standard deviation in the slope for different initializations. **(c)** Overview of all ranges used for simulations with their mean, variance, and the ratio of both, which is used to characterize the ranges.



Supplementary Figure 8: **Effects of stimuli statistics on behavior of gerbils and humans.** (a) Slope of the linear regression between stimuli and reproductions for seven gerbils (left) and six humans (right) plotted against the mean of the stimulus ranges. Vertical black markers indicate the median of slopes. Gray violin plots illustrate the distribution over all animals. Slopes for different stimulus ranges of one animal are connected by lines. Note that ranges short (red), mid (orange), long (light blue) and all (blue) differed slightly between experiments with gerbils and humans. (b) The root MSE (RMSE) of reproductions is plotted against the external variability ratio for gerbils (left) and humans (right). Vertical black markers indicate the median of RMSE. Gray violin plots illustrate the distribution over all animals. Errors for different stimulus ranges of one animal are connected by lines. Ranges correspond to those in (a). Figure courtesy of Kay Thurley and Josephine Henke.

# Programming Code

## Implementation

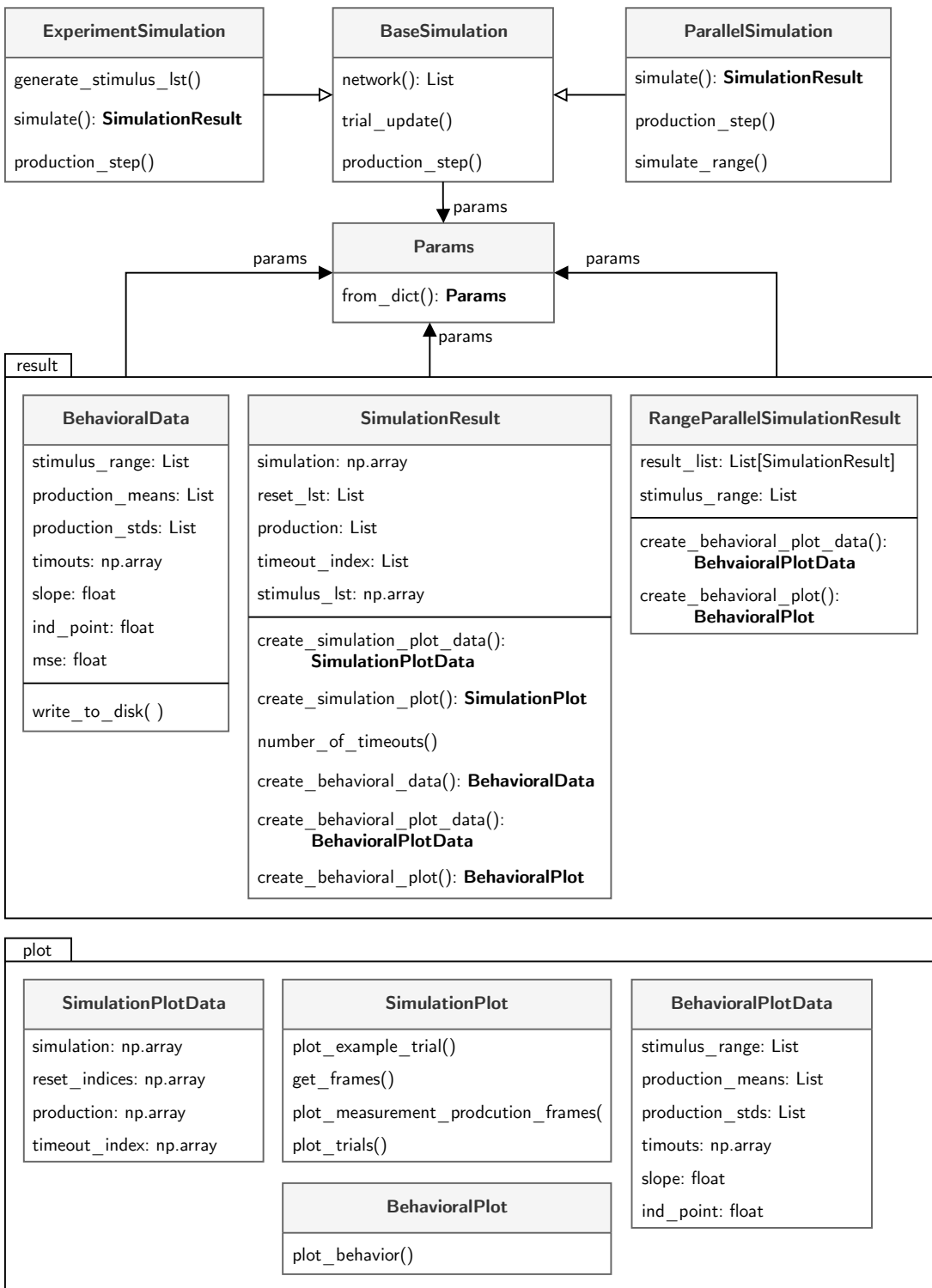
All simulations and analysis were performed with Python 3.9.7. The following libraries were used: matplotlib (3.5.1), NumPy (1.22.3), SciPy (1.8.0), and scikit-learn (1.0.2).

## Design

The code was designed in a modular way, such that multiple types of experimental procedures with shared functionality access the same basic circuit, which is implemented in `BaseSimulation`, as shown in Figure 9. The implementation of the basic circuit can be reused for all epochs. Different experiments can have different result types, all of which can be found in `result.py`. After each experiment, the results are gathered and stored together, consisting of the parameter set, the simulation time course, a list of reset time points, a list of production times, a list of indices of timeout trials and the stimulus list. Analysis of the results is performed in the same file. Depending on the analysis (e.g. behavioral), different plots are implemented in `plot.py` to visualize the results.

All parameters are set and described in `Params` and can be modified individually or by reading a parameter dictionary. The parameters configure the circuit. To initiate a simulation, the parameter set is handed to one of the implemented experiments. An interval reproduction experiment, as described in this work, is implemented in `experiment_simulation.py`. Parallel simulations of one trial (one delay, measurement, and reproduction epoch) are implemented in `parallel_simulation.py`. Both `experiment_simulation.py` and `parallel_simulation.py` contain a `simulate` function that accesses the base simulation (`BaseSimulation`) with the implementation of the basic circuit. For each epoch or update/reset step, the `simulate` function feeds the according time steps and initial conditions into the network in `BaseSimulation`. Depending on the epoch, the reset and update mechanism are turned on or off. After each epoch or pulse, the results of the network are joined to the time course of the experiment in `trial_update`. The `simulate` function returns a `SimulationResult` or `RangeParallelSimulationResult` object.

For an overview of the code structure see Figure 9 and for its usage see `simulations.ipynb` at [github.com/KatharinaBracher/MScThesis](https://github.com/KatharinaBracher/MScThesis).



Supplementary Figure 9: **Design.** The base simulation and different procedures (experiment, parallel) are all implemented in separate files. All results and analysis are collected in `result.py`, all plot for different result types are collected in `plot.py`

## References

- Acerbi, Luigi, Daniel M. Wolpert, and Sethu Vijayakumar (2012). “Internal Representations of Temporal Statistics and Feedback Calibrate Motor-Sensory Interval Timing”. *PLoS Computational Biology* 8.11. DOI: [10.1371/journal.pcbi.1002771](https://doi.org/10.1371/journal.pcbi.1002771).
- Bausenhart, Karin M., Daniel Bratzke, and Rolf Ulrich (2016). *Formation and representation of temporal reference information*. DOI: [10.1016/j.cobeha.2016.01.007](https://doi.org/10.1016/j.cobeha.2016.01.007).
- Bausenhart, Karin M., Oliver Dyjas, and Rolf Ulrich (2014). “Temporal reproductions are influenced by an internal reference: Explaining the Vierordt effect”. *Acta Psychologica* 147, pp. 60–67. DOI: [10.1016/j.actpsy.2013.06.011](https://doi.org/10.1016/j.actpsy.2013.06.011).
- Bi, Zedong and Changsong Zhou (2020). “Understanding the computation of time using neural network models”. *Proceedings of the National Academy of Sciences of the United States of America* 117.19, pp. 10530–10540. DOI: [10.1073/pnas.1921609117](https://doi.org/10.1073/pnas.1921609117).
- Block, Ned (2018). “If perception is probabilistic, why does it not seem probabilistic?” *Philosophical Transactions of the Royal Society B: Biological Sciences* 373.1755. DOI: [10.1098/rstb.2017.0341](https://doi.org/10.1098/rstb.2017.0341).
- Bubic, Andreja, D. Yves von Cramon, and Ricarda I. Schubotz (2010). “Prediction, cognition and the brain”. *Frontiers in Human Neuroscience* 4.March, pp. 1–15. DOI: [10.3389/fnhum.2010.00025](https://doi.org/10.3389/fnhum.2010.00025).
- Buhusi, Catalin V. and Warren H. Meck (2005). “What makes us tick? Functional and neural mechanisms of interval timing”. *Nature Reviews Neuroscience* 6.10, pp. 755–765. DOI: [10.1038/nrn1764](https://doi.org/10.1038/nrn1764).
- Buonomano, Dean V. (2007). “The biology of time across different scales”. *Nature Chemical Biology* 3.10, pp. 594–597. DOI: [10.1038/nchembio1007-594](https://doi.org/10.1038/nchembio1007-594).
- Buonomano, Dean V. and Uma R. Karmarkar (2002). *How do we tell time?* DOI: [10.1177/107385840200800109](https://doi.org/10.1177/107385840200800109).
- Cicchini, Guido Marco, Roberto Arrighi, Luca Cecchetti, Marco Giusti, and David C. Burr (2012). “Optimal encoding of interval timing in expert percussionists”. *Journal of Neuroscience* 32.3, pp. 1056–1060. DOI: [10.1523/JNEUROSCI.3411-11.2012](https://doi.org/10.1523/JNEUROSCI.3411-11.2012).
- Clark, Andy (2013). “Whatever next? Predictive brains, situated agents, and the future of cognitive science”. *Behavioral and Brain Sciences* 36.3, pp. 181–204. DOI: [10.1017/S0140525X12000477](https://doi.org/10.1017/S0140525X12000477).
- Cueva, Christopher J., Alex Saez, Encarni Marcos, Aldo Genovesio, Mehrdad Jazayeri, Ranulfo Romo, C. Daniel Salzman, Michael N. Shadlen, and Stefano Fusi (2020). “Low-dimensional dynamics for working memory and time

- encoding”. *Proceedings of the National Academy of Sciences of the United States of America* 117.37, pp. 23021–23032. DOI: 10.1073/pnas.1915984117.
- Dyjas, Oliver, Karin M. Bausenhart, and Rolf Ulrich (2012). “Trial-by-trial updating of an internal reference in discrimination tasks: Evidence from effects of stimulus order and trial sequence”. *Attention, Perception, and Psychophysics* 74.8, pp. 1819–1841. DOI: 10.3758/s13414-012-0362-4.
- Egger, Seth W., Nhat M. Le, and Mehrdad Jazayeri (2020). “A neural circuit model for human sensorimotor timing”. *Nature Communications* 11.1, pp. 1–14. DOI: 10.1038/s41467-020-16999-8.
- Egger, Seth W., Evan D. Remington, Chia Jung Chang, and Mehrdad Jazayeri (2019). “Internal models of sensorimotor integration regulate cortical dynamics”. *Nature Neuroscience* 22.11, pp. 1871–1882. DOI: 10.1038/s41593-019-0500-6.
- Emmons, Eric B., Benjamin J. De Corte, Youngcho Kim, Krystal L. Parker, Matthew S. Matell, and Nandakumar S. Narayanan (2017). “Rodent medial frontal control of temporal processing in the dorsomedial striatum”. *Journal of Neuroscience* 37.36, pp. 8718–8733. DOI: 10.1523/JNEUROSCI.1376-17.2017.
- Ficco, Linda, Lorenzo Mancuso, Jordi Manuello, Alessia Teneggi, Donato Liloia, Sergio Duca, Tommaso Costa, Gyula Zoltán Kovacs, and Franco Cauda (2021). “Disentangling predictive processing in the brain: a meta-analytic study in favour of a predictive network”. *Scientific Reports* 11.1, pp. 1–14. DOI: 10.1038/s41598-021-95603-5.
- Genovesio, Aldo, Satoshi Tsujimoto, and Steven P. Wise (2006). “Neuronal Activity Related to Elapsed Time in Prefrontal Cortex”. *Journal of Neurophysiology* 95.5, pp. 3281–3285. DOI: 10.1152/jn.01011.2005.
- Goel, Anubhuti and Dean V. Buonomano (2014). “Timing as an intrinsic property of neural networks: Evidence from in vivo and in vitro experiments”. *Philosophical Transactions of the Royal Society B: Biological Sciences* 369.1637. DOI: 10.1098/rstb.2012.0460.
- Grondin, Simon (2010). “Timing and time perception: A review of recent behavioral and neuroscience findings and theoretical directions”. *Attention, Perception, and Psychophysics* 72.3, pp. 561–582. DOI: 10.3758/APP.72.3.561.
- Henke, Josephine, David Bunk, Dina von Werder, Stefan Häusler, Virginia L. Flanagin, and Kay Thurley (2021). “Distributed coding of duration in rodent prefrontal cortex during time reproduction”. *eLife* 10, pp. 1–24. DOI: 10.7554/eLife.71612.
- Henke, Josphine, Virginia L. Flanagin, and Kay Thurley (2022). “A virtual reality time reproduction task for rodents”. *Frontiers in Behavioral Neuroscience* 16. DOI: 10.3389/fnbeh.2022.957804.

- Huang, Yanping and Rajesh P.N. Rao (2011). “Predictive coding”. *Wiley Interdisciplinary Reviews: Cognitive Science* 2.5, pp. 580–593. DOI: 10.1002/wcs.142.
- Issa, John B, Gilad Tocker, Michael E Hasselmo, James G Heys, and Daniel A Dombeck (2020). “Navigating Through Time: A Spatial Navigation Perspective on How the Brain May Encode Time”. *Annual Review of Neuroscience*. DOI: 10.1146/annurev-neuro-101419.
- Knill, David C. and Alexandre Pouget (2004). “The Bayesian brain: The role of uncertainty in neural coding and computation”. *Trends in Neurosciences* 27.12, pp. 712–719. DOI: 10.1016/j.tins.2004.10.007.
- Kwisthout, Johan and Iris van Rooij (2020). “Computational Resource Demands of a Predictive Bayesian Brain”. *Computational Brain and Behavior* 3.2, pp. 174–188. DOI: 10.1007/s42113-019-00032-3.
- Lewis, P. A., A. M. Wing, P. A. Pope, P. Praamstra, and R. C. Miall (2004). “Brain activity correlates differentially with increasing temporal complexity of rhythms during initialisation, synchronisation, and continuation phases of paced finger tapping”. *Neuropsychologia* 42.10, pp. 1301–1312. DOI: 10.1016/j.neuropsychologia.2004.03.001.
- Marr, D. C. and T. Poggio (1977). “From understanding computation to understanding neural circuitry”. *Neurosciences Research Program Bulletin* 15.3, pp. 470–488.
- Meirhaeghe, Nicolas, Hansem Sohn, and Mehrdad Jazayeri (2021). “A precise and adaptive neural mechanism for predictive temporal processing in the frontal cortex”. *Neuron* 109.18, 2995–3011.e5. DOI: 10.1016/j.neuron.2021.08.025.
- Mita, Akihisa, Hajime Mushiake, Keisetsu Shima, Yoshiya Matsuzaka, and Jun Tanji (2009). “Interval time coding by neurons in the presupplementary and supplementary motor areas”. *Nature Neuroscience* 12.4, pp. 502–507. DOI: 10.1038/nn.2272.
- Murakami, Masayoshi, M. Inês Vicente, Gil M. Costa, and Zachary F. Mainen (2014). “Neural antecedents of self-initiated actions in secondary motor cortex”. *Nature Neuroscience* 17.11, pp. 1574–1582. DOI: 10.1038/nn.3826.
- Patke, Alina, Michael W. Young, and Sofia Axelrod (2020). “Molecular mechanisms and physiological importance of circadian rhythms”. *Nature Reviews Molecular Cell Biology* 21.2, pp. 67–84. DOI: 10.1038/s41580-019-0179-2.
- Paton, Joseph J. and Dean V. Buonomano (2018). “The Neural Basis of Timing: Distributed Mechanisms for Diverse Functions”. *Neuron* 98.4, pp. 687–705. DOI: 10.1016/j.neuron.2018.03.045.

- Petzschner, Frederike H., Stefan Glasauer, and Klaas E. Stephan (2015). “A Bayesian perspective on magnitude estimation”. *Trends in Cognitive Sciences* 19.5, pp. 285–293. DOI: 10.1016/j.tics.2015.03.002.
- Petzschner, Frederike H., Paul Maier, and Stefan Glasauer (2012). “Combining symbolic cues with sensory input and prior experience in an iterative Bayesian framework”. *Frontiers in Integrative Neuroscience* JULY 2012. DOI: 10.3389/fnint.2012.00058.
- Rao, Rajesh P.N. and Dana H. Ballard (1999). “Predictive coding in the visual cortex: A functional interpretation of some extra-classical receptive-field effects”. *Nature Neuroscience* 2.1, pp. 79–87. DOI: 10.1038/4580.
- Remington, Evan D., Devika Narain, Eghbal A. Hosseini, and Mehrdad Jazayeri (2018). “Flexible Sensorimotor Computations through Rapid Reconfiguration of Cortical Dynamics”. *Neuron* 98.5, 1005–1019.e5. DOI: 10.1016/j.neuron.2018.05.020.
- Roxin, Alex and Anders Ledberg (2008). “Neurobiological Models of Two-Choice Decision Making Can Be Reduced to a One-Dimensional Nonlinear Diffusion Equation”. *PLoS Computational Biology* 4.3. Ed. by Lyle J. Graham, e1000046. DOI: 10.1371/journal.pcbi.1000046.
- Shi, Zhuanghua, Russell M. Church, and Warren H. Meck (2013). “Bayesian optimization of time perception”. *Trends in Cognitive Sciences* 17.11, pp. 556–564. DOI: 10.1016/j.tics.2013.09.009.
- Shima, Keisetsu and Jun Tanji (2000). “Neuronal activity in the supplementary and presupplementary motor areas for temporal organization of multiple movements”. *Journal of Neurophysiology* 84.4, pp. 2148–2160. DOI: 10.1152/jn.2000.84.4.2148.
- Sohn, Hansem, Devika Narain, Nicolas Meirhaeghe, and Mehrdad Jazayeri (2019). “Bayesian Computation through Cortical Latent Dynamics”. *Neuron* 103.5, 934–947.e5. DOI: 10.1016/j.neuron.2019.06.012.
- Straka, Hans, John Simmers, and Boris P. Chagnaud (2018). “A New Perspective on Predictive Motor Signaling”. *Current Biology* 28.5, R232–R243. DOI: 10.1016/j.cub.2018.01.033.
- Teghtsoonian, Robert and Martha Teghtsoonian (1978). “Range and regression effects in magnitude scaling”. *Perception & Psychophysics* 24.4, pp. 305–314. DOI: <https://doi.org/10.3758/BF03204247>.
- Thurley, Kay (2016). “Magnitude estimation with noisy integrators linked by an adaptive reference”. *Frontiers in Integrative Neuroscience* 10.FEB2016, pp. 1–11. DOI: 10.3389/fnint.2016.00006.
- Tsao, Albert, S. Aryana Yousefzadeh, Warren H. Meck, May Britt Moser, and Edvard I. Moser (2022). “The neural bases for timing of durations”. *Nature*

- Reviews Neuroscience* 23.11, pp. 646–665. DOI: 10.1038/s41583-022-00623-3.
- Wang, Jing, Devika Narain, Eghbal A. Hosseini, and Mehrdad Jazayeri (2018). “Flexible timing by temporal scaling of cortical responses”. *Nature Neuroscience* 21.1, pp. 102–112. DOI: 10.1038/s41593-017-0028-6.
- Wang, Xiao Jing (2002). “Probabilistic decision making by slow reverberation in cortical circuits”. *Neuron* 36.5, pp. 955–968. DOI: 10.1016/S0896-6273(02)01092-9.
- Xu, Min, Si Yu Zhang, Yang Dan, and Mu Ming Poo (2014). “Representation of interval timing by temporally scalable firing patterns in rat prefrontal cortex”. *Proceedings of the National Academy of Sciences of the United States of America* 111.1, pp. 480–485. DOI: 10.1073/pnas.1321314111.
- Zhou, Shanglin, Sotiris C. Masmanidis, and Dean V. Buonomano (2022). “Encoding time in neural dynamic regimes with distinct computational trade-offs”. *PLoS Computational Biology* 18.3, pp. 1–29. DOI: 10.1371/journal.pcbi.1009271.

Dieses Formblatt ist ausgefüllt und vom Betreuer unterschrieben als letzte Seite in das beim Prüfungsausschuss abzugebende Exemplar der Masterarbeit einzubinden.

*This form must be filled out and signed by the supervisor. It is to be included as the last page of the thesis in the copy for the examination committee.*

---

Name und Vorname  
Last name / First name

Geburtsdatum und –ort  
Birthdate / Birthplace

Titel der Arbeit  
Thesis title

Katharina Maria Bracher

24.10.1997, München

Arbeitsgruppe, in der die Arbeit angefertigt wurde  
Research group, where the work was supervised

Herz lab

PrüferIn der Arbeit  
Supervisor

Adresse des Prüfers/der Prüferin  
Address of supervisor / lab

Prof. Dr. Andreas Herz

Faculty of Biology Ludwig-Maximilians-Universität München  
Großhaderner Straße 2  
D-82152 Planegg-Martinsried

Unterschrift PrüferIn  
Signature of supervisor

Datum des Beginns der Arbeit  
Thesis start date

Datum der Abgabe der Arbeit  
Date of thesis submission

Andreas Herz Digitally signed by Andreas Herz  
Date: 2022.11.24 17:32:42  
+01'00'

18. April 2022

29. November 2022

Unterschrift des Vorsitzenden des Prüfungsausschusses  
oder eines Bevollmächtigten  
*Signature of head of examination board or representative*

**Bei Unterbrechungen / In case of postponement:**

Die Masterarbeit wurde angefertigt / The thesis was supervised

18.04.2022                    04.10.2022  
Vom / from ..... bis / to .....

04.10.2022                    29. 11.2022  
Vom / from ..... bis / to .....

Unterschrift PrüferIn/ signature or supervisor:

Andreas  
Herz

Digitally signed by  
Andreas Herz  
Date: 2022.11.24  
17:33:20 +01'00'